

Rotational flow underlying coupled surface and internal waves. I: Eulerian perspective

David Henry ^{*1}, Rossen I. Ivanov ^{†2}, and Zisis N. Sakellaris ^{‡1}

¹School of Mathematical Sciences, University College Cork, Cork, Ireland

²School of Mathematics and Statistics, Technological University Dublin,
Grangegorman Lower, Dublin, Ireland

Abstract

In this paper we examine the flow generated by coupled surface and internal small-amplitude water waves in a two-fluid layer model, where we take the upper layer to be rotational (constant vorticity) and the lower layer to be irrotational. The presence of vorticity greatly complicates the underlying analysis, yet it generates a rich array of otherwise unobservable phenomena such as the presence of critical layers, and stagnation points, in the fluid interior. We employ a phase-plane analysis to elucidate the qualitative behaviour of streamlines for a range of different coupled-wave, and vorticity, regimes. Although the water waves considered are linear in the fluid dynamics sense, the dynamical systems which govern their motion are nonlinear.

Mathematics Subject Classification (2020): 35Q35, 76B15, 37N10, 70K05.

Keywords: Internal waves, Surface waves, Vorticity, Streamlines, Phase planes.

1 Introduction

In this paper we examine the flow generated by coupled surface and internal small-amplitude water waves in a two-fluid layer model, where the upper layer is taken to be rotational (constant vorticity), while the lower layer is irrotational. This work significantly advances the recent investigations of fluid

^{*}d.henry@ucc.ie

[†]rossen.ivanov@tudublin.ie

[‡]znsakell@hotmail.com

kinematics induced by internal and surface wave motion featured in [20, 21], where both fluid layers were assumed to be irrotational. Internal water waves arise where there is a jump in density between fluid layers, which may occur when there are variations in temperature, salinity, or other fluctuations in the equations of state [29]. The two fluid-layer model is applicable when there is an internal interface which demarcates regions with a relatively significant vertical density difference: such an interface is called a pycnocline (or thermocline if the difference in densities is due to temperature variations).

The novel feature of this paper is the inclusion of vorticity in our model. Vorticity greatly complicates the mathematical analysis for the water-wave problem in general [3], primarily since the velocity field can no longer be derived from a potential function. This is particularly germane to the intricacies involved in elucidating the qualitative features of fluid motion: vorticity has a direct influence on all kinematic considerations. Incorporating (non-zero) vorticity is necessary for modelling important, and ubiquitous, physical phenomena such as wave-current interactions [3, 30]. The presence of vorticity can generate a rich array of otherwise unobservable phenomena, such as the presence of critical layers, and stagnation points, in the fluid interior, as we establish in Section 4. Note that the fluid model being considered, which consists of a rotational upper layer overlying an irrotational lower layer, also has direct physical relevance. For instance, wind-generated water waves exhibit a localised layer of vorticity near the surface. In the initial stages of wind generated-waves on the ocean, the wind “grips” the surface, producing small-amplitude water waves which subsequently develop in size [23].

Determining the underlying fluid motion generated by a wave propagating on an interface is an intriguing, and broad, area of theoretical research which has witnessed many mathematical advances over the past couple of decades. For periodic waves, a series of work initiated by the paper [11] used a phase-plane approach to investigate the underlying flow for linear irrotational surface waves on a single fluid layer: see [3, 5, 20] for additional references. This approach was extended to linear waves with constant vorticity in [16], with further subsequent investigations of the wave kinematics for single layer rotational flow such as [15], among others. Quite surprisingly, using altogether different methods, it was possible to establish a detailed picture of the underlying flow for fully nonlinear (that is, large amplitude) waves up to, and including, Stokes’ wave of extreme height [2, 4, 5, 17, 18, 24]. In short, elucidating the fine properties of individual fluid particle motion has been largely achieved for periodic surface waves.

Recently, in [20, 21] a phase-plane approach was employed to obtain a first detailed insight into flow generated by coupled surface and internal waves in the linear regime. The aim of this article is to significantly extend these

results by incorporating vorticity into our fluid model. Although the waves we study arise from a linearisation of the governing equations, the dynamical systems which prescribe the resulting fluid motion are themselves nonlinear. We apply a phase-plane analysis in order to comprehensively describe qualitative properties of the underlying wave-field kinematics for various vorticity regimes.

2 Equations of motion

We consider here a two-dimensional water flow, moving under the influence of gravity, and use a reference frame with horizontal x axis, and y axis that points vertically upwards. The water flow occupies the domain bounded below by the rigid flat bed $y = -h$, (with $h > 0$), and above by the free surface $y = \eta_1(x, t) + h_1$, the latter being a perturbation of the flat free surface $y = h_1$. Here, $h_1 > 0$ is a constant, while $\eta_1(x, t)$ is a periodic function in x of period $L > 0$ which has mean zero, that is, for all t ,

$$\int_0^L \eta_1(x, t) dx = 0.$$

The fluid is assumed to be stratified into two layers of (differing) piecewise-constant densities, and so $\rho = \rho_1$ on the upper fluid layer $\Omega_1(\eta, \eta_1)$, where

$$\Omega_1(\eta, \eta_1) := \{(x, y) : x \in [0, L], \eta(x, t) < y < h_1 + \eta_1(x, t)\},$$

while $\rho = \rho$ on the lower fluid layer $\Omega(\eta)$, where

$$\Omega(\eta) := \{(x, y) : x \in [0, L], -h < y < \eta(x, t)\}.$$

Here $y = \eta(x, t)$ denotes the internal interface separating the two fluid layers, which we also take to be periodic, $\eta(x + L, t) = \eta(x, t)$, and with zero mean,

$$\int_0^L \eta(x, t) dx = 0$$

for all t . It is assumed that the fluid is stably stratified, and so $\rho_1 < \rho \equiv (r + 1)\rho_1$ for some $r > 0$ (in an oceanographical context $r = \mathcal{O}(10^{-3})$ would typically be a reasonable value [7]). With respect to the above stratification, the velocity field can be split into

$$\mathbf{u}(x, y, t) := \begin{cases} u(x, y, t), & \text{in } \Omega(\eta), \\ u_1(x, y, t), & \text{in } \Omega_1(\eta, \eta_1), \end{cases}$$

and

$$\mathbf{v}(x, y, t) := \begin{cases} v(x, y, t), & \text{in } \Omega(\eta), \\ v_1(x, y, t), & \text{in } \Omega_1(\eta, \eta_1). \end{cases}$$

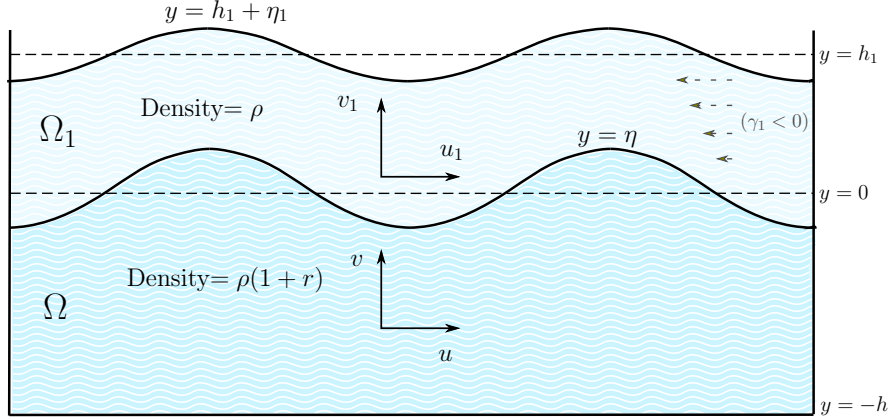


Figure 1: Coupled surface-internal water waves for $a/a_1 > 0$, and $\gamma_1 < 0$.

For ocean gravity waves it is reasonable to assume inviscid flow, whereby the equations of motion are given by the Euler equation. Working in the two-dimensional setting, the governing equations can be expressed as

$$\begin{cases} \mathbf{u}_t + \mathbf{u}\mathbf{u}_x + \mathbf{v}\mathbf{u}_y = -\frac{1}{\rho}P_x, \\ \mathbf{v}_t + \mathbf{u}\mathbf{v}_x + \mathbf{v}\mathbf{v}_y = -\frac{1}{\rho}P_y - g, \end{cases} \quad (1)$$

where $P = P(x, y, t)$ denotes the pressure, and g is the gravitational acceleration. It is also reasonable to assume incompressibility for ocean waves, and so

$$\mathbf{u}_x + \mathbf{v}_y = 0 \text{ in } \Omega \cup \Omega_1. \quad (2)$$

The vorticity of the fluid is defined to be $\boldsymbol{\gamma} = \nabla \times \mathbf{u}$, which in two-dimensions reduces to

$$\gamma_1 = u_{1,y} - v_{1,x} \text{ in } \Omega_1, \text{ while } \gamma = u_y - v_x \text{ in } \Omega. \quad (3)$$

In this paper we consider the physical regime whereby the upper fluid layer $\Omega_1(\eta, \eta_1)$ has constant (nonzero) vorticity, $\gamma_1 \neq 0$, while the lower fluid layer $\Omega(\eta)$ is irrotational, $\gamma = 0$.

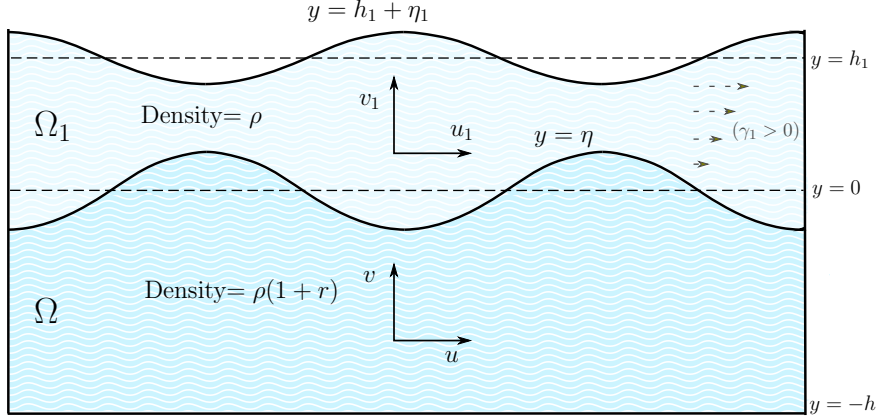


Figure 2: Coupled surface-internal water waves for $a/a_1 < 0$, and $\gamma_1 > 0$.

Complementing the equations of motion are the boundary conditions. The dynamic boundary condition

$$P = P_{atm} \text{ on } y = \eta_1(x) + h_1$$

(with P_{atm} being the constant atmospheric pressure) decouples the motion of the water from that of the air. The kinematic boundary conditions reflect the impermeability of the flat bed, the interface $y = \eta(x, t)$, and the free surface $y = h_1 + \eta_1(x, t)$, and read as

$$v_1 = \eta_{1,t} + u_1 \eta_{1,x} \text{ on } y = \eta_1(x, t) + h_1, \quad (4)$$

and

$$\begin{aligned} v_1 &= \eta_t + u_1 \eta_x & \text{on } y = \eta(x, t), \\ v &= \eta_t + u \eta_x & \text{on } y = \eta(x, t), \end{aligned} \quad (5)$$

and

$$v = 0 \text{ on } y = -h. \quad (6)$$

As a consequence of (2), the (generalized) velocity potential

$$\varphi(x, y, t) = \begin{cases} \varphi(x, y, t) & \text{in } \Omega, \\ \varphi_1(x, y, t) & \text{in } \Omega_1, \end{cases}$$

can be defined by

$$\begin{cases} u = \varphi_x, & v = \varphi_y & \text{in } \Omega, \\ u_1 = \varphi_{1,x} + \gamma_1 y, & v_1 = \varphi_{1,y} & \text{in } \Omega_1, \end{cases} \quad (7)$$

where the potential functions $\varphi(x, t)$, $\varphi_1(x, t)$ are also L -periodic in x . The kinematic boundary conditions (4) and (5) can now be reexpressed as

$$\eta_{1,t} = (\varphi_{1,y})_{s_1} - \eta_{1,x}[(\varphi_{1,x})_{s_1} + \gamma_1(h_1 + \eta_1)] \quad (8)$$

and

$$\eta_t = (\varphi_{1,y})_s - \eta_x[(\varphi_{1,x})_s + \gamma_1\eta], \quad \eta_t = (\varphi_y)_s - \eta_x(\varphi_x)_s,$$

where the subscript s_1 denotes the trace of the involved functions on the free surface $y = \eta_1(x, t) + h_1$, while the subscript s denotes the trace on the interface $y = \eta(x, t)$. In the following we denote

$$\begin{aligned} \Phi(x, t) &= \varphi(x, \eta(x, t), t), & \Phi_1(x, t) &= \varphi_1(x, \eta(x, t), t), \\ \Phi_2(x, t) &= \varphi_1(x, h_1 + \eta_1(x, t), t). \end{aligned} \quad (9)$$

3 Linear approximation of the equations

3.1 Hamiltonian formulation

The governing equations (1)–(6) can be linearised by considering their Hamiltonian formulation, where the Hamiltonian functional for our physical set-up is given by the total energy

$$H = \int \int_{\Omega \cup \Omega_1} \rho \left\{ \frac{\mathbf{u}^2 + \mathbf{v}^2}{2} + gy \right\} dy dx.$$

The Hamiltonian, H , is given by the energy of the system for one period (that is, over horizontal length L). The Hamiltonian density of the Hamiltonian functional can be written explicitly by following an approach based on Dirichlet-Neumann (DN) operators, see [13]. A detailed account of the Hamiltonian formulation for the more complicated setting of constant (non-zero) vorticity in each layer is available in [7, 8] (however note that an integral density is used in these works since solutions are considered over the entire real-line).

In order to obtain a systematic linearisation of the governing equations we perform a suitable nondimensionalisation and scaling of the variables. To simplify the derivation process, we make the assumption that the depths h and h_1 are roughly of the same order of magnitude, so we can introduce a depth scale \mathfrak{h} such that $h, h_1 = \mathcal{O}(\mathfrak{h})$; similarly for the amplitudes of the surface and internal wave, a and a_1 , respectively — we introduce the amplitude length scale \mathfrak{a} and assume that $a, a_1 = \mathcal{O}(\mathfrak{a})$. Defining the dimensionless parameters

$$\epsilon = \mathfrak{a}/\mathfrak{h}, \quad \delta = k\mathfrak{h}, \quad \mathfrak{e} = \mathfrak{a}k$$

where $k = 2\pi/L > 0$ is the wavenumber, it follows that ϵ measures the amplitude size relative to the layer depth, δ measures the depth relative to the wavelength, while ϵ is the *wave steepness* parameter. In the linear regime it is necessary for both ϵ and ϵ to be very small ($\ll 1$), while for the time being we can assume that $\delta = \mathcal{O}(1)$. These parameters can be used to nondimensionalise all quantities along classical lines (cf. [22])

$$\begin{aligned}\bar{h} &= \mathfrak{h}h, & \bar{h}_1 &= \mathfrak{h}h_1, & \bar{x} &= \frac{\mathfrak{h}}{\delta}x, & \bar{y} &= \frac{\mathfrak{h}}{\delta^2}y, & \bar{t} &= \frac{\mathfrak{h}}{\delta\sqrt{\bar{g}\mathfrak{h}}}t, & \bar{\eta} &= \epsilon\mathfrak{h}\eta, \\ \bar{\varphi} &= \frac{\epsilon}{\delta}\mathfrak{h}\sqrt{\bar{g}\mathfrak{h}}\varphi, & \bar{\gamma}_1 &= \frac{\sqrt{\bar{g}\mathfrak{h}}}{\mathfrak{h}}\gamma_1, & \bar{\eta}_1 &= \epsilon\mathfrak{h}\eta_1, & \bar{\varphi}_1 &= \frac{\epsilon}{\delta}\mathfrak{h}\sqrt{\bar{g}\mathfrak{h}}\varphi_1.\end{aligned}$$

Here the dimensional quantities are those with a bar, while the nondimensional ones are without. The nondimensional version of the Earth's acceleration $\bar{g} = 9.81 \text{ m/s}^2$ is $g = 1$, but we will retain g throughout the following in order to easily revert back to the dimensional form of the governing equations. Then equations (8)–(9) become (for the non-dimensional variables)

$$\eta_{1,t} = (\varphi_{1,y})_{s_1} - \eta_{1,x}[\epsilon(\varphi_{1,x})_{s_1} + \gamma_1(h_1 + \epsilon\eta_1)] \quad (10)$$

$$\begin{aligned}\eta_t &= (\varphi_{1,y})_s - \epsilon\eta_x[(\varphi_{1,x})_s + \gamma_1\eta], & \eta_t &= (\varphi_y)_s - \epsilon\eta_x(\varphi_x)_s, \\ \Phi(x, t) &= \varphi(x, \epsilon\eta(x, t), t), & \Phi_1(x, t) &= \varphi_1(x, \epsilon\eta(x, t), t), \\ \Phi_2(x, t) &= \varphi_1(x, h_1 + \epsilon\eta_1(x, t), t).\end{aligned} \quad (11)$$

In the leading order, as $\epsilon \rightarrow 0$, equations (10)–(11) are approximated by

$$\eta_{1,t} = (\varphi_{1,y})_{s_1} - \gamma_1 h_1 \eta_{1,x}, \quad (12)$$

$$\eta_t = (\varphi_{1,y})_s, \quad \eta_t = (\varphi_y)_s, \quad (13)$$

and

$$\Phi(x, t) = \varphi(x, 0, t), \quad \Phi_1(x, t) = \varphi_1(x, 0, t), \quad \Phi_2(x, t) = \varphi_1(x, h_1, t).$$

The resulting Hamiltonian variables are η, η_1 and

$$\begin{aligned}\xi &= \frac{\rho\varphi(x, 0, t) - \rho_1\varphi_1(x, 0, t)}{\rho_1} \equiv (r + 1)\Phi(x, t) - \Phi_1(x, t), \\ \xi_1 &= \varphi_1(x, h_1, t) \equiv \Phi_2(x, t).\end{aligned} \quad (14)$$

With the nondimensionalisation and scaling introduced above, and ignoring the linear terms (whose average is 0), the Hamiltonian admits an expansion of the form

$$\frac{\bar{H}}{\rho_1\bar{g}\mathfrak{h}^3} = H(\xi, \xi_1, \eta, \eta_1) = \epsilon^2 H^{(2)}(\xi, \xi_1, \eta, \eta_1) + \epsilon^3 H^{(3)}(\xi, \xi_1, \eta, \eta_1) + \dots \quad (15)$$

The leading order term is (see formula (4.15) in [7] with $\gamma = 0$)

$$\begin{aligned} H^{(2)}(\xi, \xi_1, \eta, \eta_1) = & \frac{1}{2} \int_0^L \left[\xi \frac{D \tanh(hD) \coth(h_1 D)}{(r+1) \coth(h_1 D) + \tanh(hD)} \xi \right. \\ & + 2\xi \frac{D \tanh(hD) \operatorname{csch}(h_1 D)}{(r+1) \coth(h_1 D) + \tanh(hD)} \xi_1 + \xi_1 \frac{D [\tanh(hD) \coth(h_1 D) + r+1]}{(r+1) \coth(h_1 D) + \tanh(hD)} \xi_1 \\ & \left. + gr\eta^2 + (g + \gamma_1^2 h_1) \eta_1^2 - 2\gamma_1 h_1 \xi_1 \eta_{1,x} \right] dx, \end{aligned}$$

where the operator D is defined as $D = -i\partial_x$. The corresponding Hamiltonian equations have the form (cf. [7, 8])

$$\begin{aligned} \epsilon^2 \xi_t &= -\frac{\delta H}{\delta \eta} - \Gamma \int_0^x \frac{\delta H}{\delta \xi(x')} dx', & \epsilon^2 \eta_t &= \frac{\delta H}{\delta \xi} \\ \epsilon^2 \xi_{1,t} &= -\frac{\delta H}{\delta \eta_1} - \Gamma_1 \int_0^x \frac{\delta H}{\delta \xi_1(x')} dx', & \epsilon^2 \eta_{1,t} &= \frac{\delta H}{\delta \xi_1} \end{aligned}$$

where $\Gamma = -\gamma_1$, $\Gamma_1 = \gamma_1 = -\Gamma$ are constants. At the leading order, $H = \epsilon^2 H^{(2)}$, these equations are linear, and integration is replaced by ∂_x^{-1} , giving

$$\begin{aligned} \xi_t &= -gr\eta - \Gamma \partial_x^{-1} \eta_t, \\ \eta_t &= \frac{D \tanh(hD) \coth(h_1 D)}{(r+1) \coth(h_1 D) + \tanh(hD)} \xi \\ &\quad + \frac{D \tanh(hD) \operatorname{csch}(h_1 D)}{(r+1) \coth(h_1 D) + \tanh(hD)} \xi_1, \quad (16) \\ \xi_{1,t} &= -\gamma_1 h_1 \xi_{1,x} - (g + \gamma_1^2 h_1) \eta_1 - \Gamma_1 \partial_x^{-1} \eta_{1,t}, \\ \eta_{1,t} &= -\gamma_1 h_1 \eta_{1,x} + \frac{D \tanh(hD) \operatorname{csch}(h_1 D)}{(r+1) \coth(h_1 D) + \tanh(hD)} \xi \\ &\quad + \frac{D [\tanh(hD) \coth(h_1 D) + r+1]}{(r+1) \coth(h_1 D) + \tanh(hD)} \xi_1. \end{aligned}$$

These equations will be used later to relate the boundary values of the potentials on the surface and the internal interface and to obtain matching conditions, which will lead to a definition (22) of the parameter A , and to the dispersion relation for our system.

3.2 Wave solutions

The aim now is to explicitly determine the velocity potentials in the body of the fluid from their values on the surface and on the interface. Essentially, this procedure is as an analytic continuation based on the fact that the

potentials satisfy the Laplace equation inside the fluid, which follows from (2), (3) and (7). The boundary values will be obtained from the linear equations (in the leading order) that relate them to η_t and $\eta_{1,t}$, namely (12) and (13). The relevant boundary value problem for the lower layer is

$$\begin{aligned}\Delta\varphi(x, y) &= 0, \\ \frac{\partial\varphi}{\partial\mathbf{n}} &= 0 \text{ on } y = -h, \\ \varphi_y(x, 0, t) &= \eta_t(x, t),\end{aligned}\tag{17}$$

where \mathbf{n} denotes the outward pointing unit normal, and differentiation represents the normal derivative. In our considerations it must be taken into account that, in the periodic case, the set of eigenvalues of the operator $D = -i\partial_x$ is discrete. Indeed, the operator D now has eigenvalues $\tilde{k} = \tilde{k}_n = \frac{2\pi n}{L}$ for any integer n , and periodic eigenfunctions $e^{i\tilde{k}x}$, since

$$De^{i\tilde{k}x} = \tilde{k}e^{i\tilde{k}x}.$$

For convenience, summation over the integers n (from $-\infty$ to ∞) will be written as summation over \tilde{k} . The dependence on t is not written explicitly (we can treat t here as a parameter) and the problem is stated in the (x, y) domain. The general solution in the bulk is a superposition of harmonic functions $\varphi_{\tilde{k}}(x, y)$, periodic in x , satisfying (17):

$$\varphi(x, y) = \sum_{\tilde{k}} \mathcal{A}(\tilde{k}) \varphi_{\tilde{k}}(x, y), \quad \varphi_{\tilde{k}}(x, y) = e^{i\tilde{k}x} \cosh[\tilde{k}(y + h)].$$

The as yet unknown function $\mathcal{A}(\tilde{k})$ can be obtained from the interface condition

$$\eta_t(x) = \varphi_y(x, 0) = \sum_{\tilde{k}} \tilde{k} \mathcal{A}(\tilde{k}) e^{i\tilde{k}x} \sinh(\tilde{k}h).$$

The Fourier coefficient of the above expansion is given by

$$\begin{aligned}\mathcal{A}(\tilde{k}) &= \frac{1}{L \tilde{k} \sinh(\tilde{k}h)} \int_0^L e^{-i\tilde{k}x'} \eta_t(x') dx', \\ \varphi(x, y) &= \frac{1}{L} \sum_{\tilde{k}} \int_0^L e^{i\tilde{k}(x-x')} \eta_t(x') \frac{\cosh[\tilde{k}(y + h)]}{\tilde{k} \sinh(\tilde{k}h)} dx'.\end{aligned}$$

The periodic delta-function

$$\delta(x - x') = \frac{1}{L} \sum_{\tilde{k}} e^{i\tilde{k}(x-x')}$$

is normalised by the condition $\int_0^L \delta(x)dx = 1$ and we have

$$\varphi(x, y) = \frac{\cosh[D(y + h)]}{D \sinh(Dh)} \int_0^L \frac{1}{L} \sum_{\tilde{k}} e^{i\tilde{k}(x-x')} \eta_t(x') dx' = \frac{\cosh[D(y + h)]}{D \sinh(Dh)} \eta_t(x).$$

The Ansatz which is typically invoked for linear water waves is

$$\eta = a \cos(kx - \omega t), \quad \eta_1 = a_1 \cos(kx - \omega t), \quad (18)$$

and, for such sinusoidal η and η_1 , we note that the action of ‘ D ’ may be formally replaced by multiplication with ‘ k ’ for operators which involve only even orders of D . Therefore

$$\varphi(x, y, t) = ac(k) \frac{\cosh[k(y + h)]}{\sinh(kh)} \sin(kx - \omega t), \quad (19)$$

and also

$$\Phi(x, t) := \varphi(x, 0, t) = ac \coth(kh) \sin(kx - \omega t), \quad (20)$$

where

$$c(k) = \frac{\omega(k)}{k}$$

is the phasespeed of the wave. The boundary-value problem in the upper layer is

$$\begin{aligned} \Delta \varphi_1(x, y) &= 0, \\ \varphi_{1,y}(x, h_1) &= \eta_{1,t}(x) + \gamma_1 h_1 \eta_{1,x} \text{ on } y = h_1, \\ \varphi_{1,y}(x, 0) &= \eta_t(x). \end{aligned}$$

The general solution in the bulk is a superposition of harmonic functions of the form $e^{\pm \tilde{k}y + i\tilde{k}x}$, periodic in x , that is

$$\varphi_1(x, y) = \sum_{\tilde{k}} \left(\mathcal{A}(\tilde{k}) e^{\tilde{k}y + i\tilde{k}x} + \mathcal{B}(\tilde{k}) e^{-\tilde{k}y + i\tilde{k}x} \right).$$

The as yet unknown Fourier coefficients $\mathcal{A}(\tilde{k})$ and $\mathcal{B}(\tilde{k})$ can be obtained from the surface and interface conditions

$$\begin{aligned} \eta_{1,t} + \gamma_1 h_1 \eta_{1,x} &= \varphi_{1,y}(x, h_1) = \sum_{\tilde{k}} e^{i\tilde{k}x} \tilde{k} \left(\mathcal{A}(\tilde{k}) e^{\tilde{k}h_1} - \mathcal{B}(\tilde{k}) e^{-\tilde{k}h_1} \right), \\ \eta_t &= \varphi_{1,y}(x, 0) = \sum_{\tilde{k}} e^{i\tilde{k}x} \tilde{k} \left(\mathcal{A}(\tilde{k}) - \mathcal{B}(\tilde{k}) \right). \end{aligned}$$

Evaluating the coefficients of the Fourier series given above allows us to determine $\mathcal{A}(\tilde{k})$ and $\mathcal{B}(\tilde{k})$:

$$\begin{aligned}\mathcal{A}(\tilde{k}) &= \frac{1}{L} \int_0^L e^{-i\tilde{k}x'} \frac{[\eta_{1,t}(x') + \gamma_1 h_1 \eta_{1,x}(x')] - e^{-\tilde{k}h_1} \eta_t(x')}{2\tilde{k} \sinh(\tilde{k}h_1)} dx', \\ \mathcal{B}(\tilde{k}) &= \frac{1}{L} \int_0^L e^{-i\tilde{k}x'} \frac{[\eta_{1,t}(x') + \gamma_1 h_1 \eta_{1,x}(x')] - e^{\tilde{k}h_1} \eta_t(x')}{2\tilde{k} \sinh(\tilde{k}h_1)} dx',\end{aligned}$$

and proceeding as in the solution of the previous problem we obtain finally

$$\varphi_1(x, y) = \frac{\cosh(yD)}{D \sinh(h_1 D)} [\eta_{1,t}(x) + \gamma_1 h_1 \eta_{1,x}(x)] - \frac{\cosh((y - h_1)D)}{D \sinh(h_1 D)} \eta_t(x),$$

which the Ansatz (18) gives

$$\varphi_1(x, y, t) = a_1 \mathfrak{c} \{ \sinh k(y - h_1) + A \cosh k(y - h_1) \} \sin(kx - \omega t) \quad \text{in } 0 < y < h_1, \quad (21)$$

for

$$\mathfrak{c} = c - \gamma_1 h_1$$

and

$$A := -\frac{a}{a_1} \frac{c}{\mathfrak{c} \sinh kh_1} + \frac{\cosh kh_1}{\sinh kh_1}. \quad (22)$$

Remark 3.1. *The quantity \mathfrak{c} measures the speed of the sheared current at the surface of the upper layer relative to the phasespeed of the wave. The sign of $c \cdot \mathfrak{c}$ is linked to the appearance of critical layers. The Rayleigh equation for linear fluid flow in the upper-layer is*

$$(\gamma_1 y - c) (-\tilde{v}''(y) + k^2 \tilde{v}(y)) = 0,$$

and this equation becomes singular if $\gamma_1 y^{crit} = c$ for some value $y^{crit} \in (0, h_1)$, near which depth critical layers occur. Thus, critical layers occur in the upper fluid layer if and only if $c \cdot \mathfrak{c} < 0$. In the setting of a single fluid layer, it was first observed by Kelvin that streamlines resembling cat's eye patterns form near the critical layer; we show in Section 4 below that a similar phenomenon occurs also in the two-fluid layer setting near such critical values.

On the boundaries of the upper domain we have

$$\begin{aligned}\Phi_1(x, t) &:= \varphi_1(x, 0, t) = a_1 \mathfrak{c} [-\sinh(kh_1) + A \cosh(kh_1)] \sin(kx - \omega t), \\ \Phi_2(x, t) &:= \varphi_1(x, h_1, t) = a_1 \mathfrak{c} A \sin(kx - \omega t),\end{aligned} \quad (23)$$

and substituting (18) into the first and the third equations of (16) gives

$$\xi = \frac{a}{kc} (gr + \gamma_1 c) \sin(kx - \omega t), \quad \xi_1 = \frac{a_1 [g - \gamma_1 \mathfrak{c}]}{k\mathfrak{c}} \sin(kx - \omega t). \quad (24)$$

Recalling the definition of Hamiltonian variables (14), (20) and (23) gives

$$\xi = [(r + 1)ac \coth(kh) - a_1 \mathfrak{c}(-\sinh(kh_1) + A \cosh(kh_1))] \sin(kx - \omega t),$$

and comparison with (24) leads to

$$[(r + 1)ac \coth(kh) - a_1 \mathfrak{c}(-\sinh(kh_1) + A \cosh(kh_1))] = \frac{a}{kc} [gr + \gamma_1 \mathfrak{c}]. \quad (25)$$

From (14), (23) and (24) we obtain an expression for A with no explicit dependence on a/a_1 :

$$A = \frac{g - \gamma_1 \mathfrak{c}}{k\mathfrak{c}^2}. \quad (26)$$

Remark 3.2. *The nondimensional parameter A plays a key role in determining the qualitative features of the resulting fluid motion. In [20, 21] it was shown that in the irrotational setting ($\gamma_1 = 0$) the parameter ranges $0 < A < 1$, $A = 1$, and $A > 1$ prescribe regimes with qualitatively different underlying flow kinematics. However, recently in [19], it was proven that A can, in fact, never be less than 1 in the irrotational setting. In the rotational setting considered herein, A can take values in the ranges $A > 1$, $A = 1$, and $0 < A < 1$, and indeed it follows from (66) that A may also take negative values. Discussion of the asymptotic behaviour of A is given in the Appendix.*

Lemma 3.1. (i) *For $\gamma_1 \leq 0$, then $A > 0$ is strictly positive.*

(ii) *For $\gamma_1 > 0$ and $c < \gamma_1 h_1$ ($\mathfrak{c} < 0$), then $A > 0$.*

(iii) *For $\gamma_1 > 0$, $c > \gamma_1 h_1$ ($\mathfrak{c} > 0$), and $c^2 < 4gh_1$, then $A > 0$.*

(iv) *For $\gamma_1 > 0$, $c > \gamma_1 h_1$ ($\mathfrak{c} > 0$), and $4gh_1 \leq c^2$, then $A \leq 0$ is non-positive.*

Proof. The proof of the first two parts follows immediately from (66), since $k > 0$. For part (iii) we note that (66) implies that A has the same sign as $\gamma_1^2 h_1 - \gamma_1 c + g$, and this is strictly positive if $c^2 < 4gh_1$. Part (iv) follows by noting that this quadratic in γ_1 is negative if $c^2 > 4gh_1$, since we assume that $c > \gamma_1 h_1$. (Note that $4g < \gamma_1 c$ implies that $c^2 > 4gh_1$, for $c > \gamma_1 h_1$.) Relation (66), regarded as a quadratic in \mathfrak{c} , has real-valued solutions if and only if $A \geq -\frac{\gamma_1^2}{4gk}$, which serves as a lower bound for the parameter A . \square

It is useful for later reference to reexpress (22) as

$$\frac{a}{a_1} \frac{c}{\mathfrak{c}} = \cosh kh_1 - A \sinh kh_1 = \frac{1 - A}{2} e^{kh_1} + \frac{1 + A}{2} e^{-kh_1} \quad (27)$$

where the right-hand side is a strictly decreasing function of A . From (66) and (27) we obtain

$$\frac{a}{a_1} = \frac{\mathfrak{c}}{c} \sinh(kh_1) \left(\coth(kh_1) - \frac{g - \gamma_1 \mathfrak{c}}{k \mathfrak{c}^2} \right). \quad (28)$$

Regarding (28) as a quadratic in \mathfrak{c} then, if $\frac{a}{a_1} \frac{c}{\mathfrak{c}} > 0$,

$$-\frac{\gamma_1 \tanh kh_1}{2k} + \frac{\sqrt{\gamma_1^2 \tanh^2 kh_1 + 4gk \tanh kh_1}}{2k} < \mathfrak{c},$$

for $c > \gamma_1 h_1$ ($\mathfrak{c} > 0$), while

$$\mathfrak{c} < -\frac{\gamma_1 \tanh kh_1}{2k} - \frac{\sqrt{\gamma_1^2 \tanh^2 kh_1 + 4gk \tanh kh_1}}{2k},$$

for $c < \gamma_1 h_1$ ($\mathfrak{c} < 0$). When $\frac{a}{a_1} \frac{c}{\mathfrak{c}} < 0$, there is a reversal of sign in the above inequalities. In the presence of a critical layer ($c/\mathfrak{c} < 0$), if $a/a_1 < 0$ then

$$\gamma_1 > \sqrt{\frac{g \tanh kh_1}{kh_1^2 - h_1 \tanh kh_1}},$$

as can be seen from the second inequality for \mathfrak{c} above. It is interesting to note that this expression matches the necessary and sufficient condition that ensures the existence of critical layers in the one fluid layer setting, cf [10, 14]. From (25) and (66) we have

$$\begin{aligned} a \left((r+1)c \coth(kh) - \frac{gr}{kc} - \frac{\gamma_1}{k} \right) \\ = a_1 \mathfrak{c} \left(-\sinh(kh_1) + \frac{g - \gamma_1 \mathfrak{c}}{k \mathfrak{c}^2} \cosh(kh_1) \right). \end{aligned} \quad (29)$$

3.3 Dispersion relation

Relations (28) and (29) can be used to obtain two different expressions for the ratio of amplitude parameters a/a_1 : equating these expressions results in the dispersion relation

$$P_4(c) := \left(1 + \frac{1+r}{\tanh kh \tanh kh_1} \right) c^4 - \gamma_1 h_1 \left[2 + \frac{1+r}{\tanh kh} \left(\frac{2}{\tanh kh_1} - \frac{1}{kh_1} \right) \right] c^3$$

$$\begin{aligned}
& - \left[\frac{g(1+r)}{k} \left(\frac{1}{\tanh kh_1} + \frac{1}{\tanh kh} \right) \right. \\
& \quad \left. + (\gamma_1 h_1)^2 \left\{ \left(\frac{1}{kh_1} + \frac{1+r}{\tanh kh} \right) \left(\frac{1}{kh_1} - \frac{1}{\tanh kh_1} \right) - 1 \right\} \right] c^2 \\
& - \frac{\gamma_1 h_1}{k} \left[\gamma_1^2 h_1 \left(\frac{1}{\tanh kh_1} - \frac{1}{kh_1} \right) + g \left(\frac{r-1}{kh_1} - \frac{2r}{\tanh kh_1} \right) \right] c \\
& \quad - r \frac{g}{k} \left[(\gamma_1 h_1)^2 \left(\frac{1}{\tanh kh_1} - \frac{1}{kh_1} \right) - \frac{g}{k} \right] = 0. \quad (30)
\end{aligned}$$

A detailed discussion of the roots of this equation, and the corresponding wave solutions, in the context of equatorial wave-current interactions can be found in [7].

Remark 3.3. *When $r \rightarrow 0$, the two layers have the same density. Disregarding the zero solution, $c = 0$, the dispersion relation will degenerate to a cubic equation, namely*

$$\begin{aligned}
& [-kc(\coth kh_1 + \coth kh) + \gamma_1] (k\mathfrak{c}^2 \coth kh_1 + \gamma_1 \mathfrak{c} - g) \\
& \quad + \frac{1}{\sinh^2 kh_1} k^2 \mathfrak{c}^2 c = 0.
\end{aligned}$$

This matches the cubic dispersion relation in [25], which is also posed in terms of \mathfrak{c} , following various rearrangements of terms.

Remark 3.4. *In the limit where the lower layer is infinitely more dense than the upper one, $r \rightarrow \infty$, the dispersion relation is reduced to:*

$$(-kc^2 \coth kh + g) (k\mathfrak{c}^2 \coth kh_1 + \gamma_1 \mathfrak{c} - g) = 0,$$

with solutions $c_1^2 = \frac{g \tanh kh}{k}$ and $\mathfrak{c}_1^\pm = -\frac{\gamma_1 \tanh kh_1}{2k} \pm \frac{\sqrt{\gamma_1^2 \tanh^2 kh_1 + 4gk \tanh kh_1}}{2k}$.

Remark 3.5. *Taking the limit $a \rightarrow 0$, the upper-layer now has just one nontrivial free-boundary. In particular, $A = \coth kh_1$ and (66), (29) imply that either $\mathfrak{c} = 0$ ($c = \gamma_1 h_1$) or else*

$$c = \frac{1}{2k} \left[\gamma_1 (2kh_1 - \tanh kh_1) \pm \sqrt{\gamma_1^2 \tanh^2 kh_1 + 4kg \tanh kh_1} \right].$$

This matches the dispersion relation for waves propagating on a single homogeneous fluid layer, in the presence of a sheared background current [9].

Remark 3.6. *The dispersion relation (30) is invariant under the transformation $(c, \gamma_1) \mapsto (-c, -\gamma_1)$.*

When the constant term of the quartic equation (30) representing the dispersion relation is negative, we have at least two real roots, in view of the positivity of the leading order coefficient. Thus, for γ_1, h_1, k such that

$$\left[(\gamma_1 h_1)^2 \left(\frac{1}{\tanh kh_1} - \frac{1}{kh_1} \right) - \frac{g}{k} \right] > 0 \iff \frac{\tanh kh_1}{kh_1} < \frac{\gamma_1^2 h_1}{g + \gamma_1^2 h_1},$$

we have at least two real solutions. Returning to (28), we obtain two amplitude ratios as well, provided that $c \neq 0$. From Vieta's formulas [28], the product of all the roots of (30) is proportional to

$$-r \frac{g}{k} \left(\frac{\tanh kh \tanh kh_1}{\tanh kh \tanh kh_1 + 1 + r} \right) \left[\gamma_1^2 h_1 \left(\frac{kh_1 - \tanh kh_1}{k \tanh kh_1} \right) - \frac{g}{k} \right].$$

Remark 3.7. *In the long wave regime, we can assume that the coefficient of the quadratic term in (30) is negative, that is, that the following inequality holds true:*

$$\begin{aligned} & \frac{g(1+r)}{k} \left(\frac{1}{\tanh kh_1} + \frac{1}{\tanh kh} \right) \\ & + (\gamma_1 h_1)^2 \left\{ \left(\frac{1}{kh_1} + \frac{1+r}{\tanh kh} \right) \left(\frac{1}{kh_1} - \frac{1}{\tanh kh_1} \right) - 1 \right\} > 0. \end{aligned}$$

Indeed, under the long wave assumption, we have $\tanh kh_1 \approx kh_1$, whereas $\frac{g}{k} \gg 1$. In that setting, the quadratic expression

$$\begin{aligned} P_4''(c) &= 12 \left(1 + \frac{1+r}{\tanh kh \tanh kh_1} \right) c^2 \\ &- 6\gamma_1 h_1 \left[2 + \frac{1+r}{\tanh kh} \left(\frac{2}{\tanh kh_1} - \frac{1}{kh_1} \right) \right] c - 2 \left[\frac{g(1+r)}{k} \left(\frac{1}{\tanh kh_1} + \frac{1}{\tanh kh} \right) \right. \\ &\left. + (\gamma_1 h_1)^2 \left\{ \left(\frac{1}{kh_1} + \frac{1+r}{\tanh kh} \right) \left(\frac{1}{kh_1} - \frac{1}{\tanh kh_1} \right) - 1 \right\} \right] \end{aligned}$$

will have two distinct real roots, which we denote by c_1'', c_2'' , that can be written down explicitly. If the condition $P_4'(c_1)P_4'(c_2) > 0$ holds true, then the equation $P_4'(c) = 0$ has at most one real solution. Thus, we can infer whether (30) has simple real solutions. On the other hand, a condition like $\frac{\tanh kh_1}{kh_1} < \frac{\gamma_1^2 h_1}{g + \gamma_1^2 h_1}$ can only hold for $\gamma_1 \gg g/h_1$ in the long wave setting.

Remark 3.8. For $\gamma_1 = 0$, the dispersion relation (30) reduces to that of a system of coupled surface and internal waves above a flat bed:

$$\left[1 + \frac{1+r}{\tanh kh \tanh kh_1} \right] c^4 - \left[\frac{g(1+r)}{k} \left(\frac{1}{\tanh kh_1} + \frac{1}{\tanh kh} \right) \right] c^2 + r \frac{g^2}{k^2} = 0,$$

see [20].

Remark 3.9. When $k \ll 1$, we can approximate $\tanh kh \approx kh$, $\tanh kh_1 \approx kh_1$, so that

$$c^4 - \gamma_1 h_1 c^3 - g(h + h_1)c^2 + \gamma_1 h h_1 g c + \frac{r g^2 h h_1}{1 + r} \approx 0,$$

a relation also derived in [7].

The remainder of this paper is concerned with determining qualitative properties of the fluid motion which is prescribed by the above wave solutions, by subjecting the relevant dynamical systems to a phase plane analysis. We do not address matters concerning the generation, or stability (see, for instance, [1]), of such wave solutions.

4 Phase plane analysis

Explicit expressions for the velocity fields induced by the linear wave Ansatz (18) in the lower, and upper, fluid layers can be obtained directly from (7), (19) and (21). If $(x(t), y(t))$ is the path of a particle in the lower-fluid layer Ω , then the motion of the particle is described by the nonlinear nonautonomous dynamical system

$$\begin{cases} \frac{dx}{dt} = u = a\omega \cos(kx - \omega t) \frac{\cosh k(y + h)}{\sinh kh} \\ \frac{dy}{dt} = v = a\omega \sin(kx - \omega t) \frac{\sinh k(y + h)}{\sinh kh}, \end{cases} \quad (31a)$$

for $-h < y < 0$, with initial data (x_0, y_0) . In the upper-fluid layer Ω_1 , particle trajectories $(x(t), y(t))$ are prescribed by the nonlinear nonautonomous dynamical system

$$\begin{cases} \frac{dx}{dt} = a_1 k \mathfrak{c} \cos(kx - \omega t) \{ \sinh k(y - h_1) + A \cosh k(y - h_1) \} + \gamma_1 y \\ \frac{dy}{dt} = a_1 k \mathfrak{c} \sin(kx - \omega t) \{ \cosh k(y - h_1) + A \sinh k(y - h_1) \}, \end{cases} \quad (31b)$$

for $0 < y < h_1$, with initial data (x_0, y_0) . The mean-level of the oscillating internal wave interface $y = \eta$ is located at $y = 0$, whereas the free-surface $y = h_1 + \eta_1$ oscillates about the mean-level located at $y = h_1$. The right-hand sides of the differential systems (31a) and (31b) are smooth, therefore the existence of unique local smooth solutions is ensured by the Picard–Lindelöf theorem [26]. Furthermore, since y is bounded, the right-hand sides

of (31a) and (31b) are bounded, hence these unique solutions are defined globally [26]. The right-hand sides of both (31a) and (31b) are nonlinear, and thus such systems cannot be solved explicitly. Rather than linearising the dynamical systems (31a) and (31b), we will analyse the fully nonlinear dynamical systems by way of phase plane methods, thereby establishing the salient qualitative features of the flow prescribed by both (31a) and (31b). Since the fluid layers are separated by an impermeable interface $y = \eta(x, t)$, and the solutions (19) and (21) satisfy the matching conditions (13) at this interface by design, we can address the phase plane analysis of system (31a) in the lower-fluid layer Ω , and system (31b) in the upper-fluid layer Ω_1 , separately in the first instance, and then piece together the information to get a picture of the motion of the entire two-layer body.

For the purposes of performing a phase-plane analysis of the nonlinear dynamical systems (31a) and (31b), without loss of generality we can restrict our attention to waves for which $c > 0$, noting from Remark (3.6) that if c is a wavespeed prescribed by the dispersion relation (30) for γ_1 , then $-c$ will be a solution of (30) for the vorticity $-\gamma_1$. We shall regard the wavenumber k and frequency ω (and hence $c = \omega/k$) as fixed for a given wave motion, and determine the qualitative features of the motion which results from varying the vorticity γ_1 , and the nondimensional parameter A (see Remark 3.2 and Lemma 3.1). (Of course, for a given coupled-wave motion, γ_1 and A are not free-parameters, and neither are k and ω fixed but, rather, their values are interlinked and specified by the dispersion relation (30).) Using this approach we obtain qualitative descriptions of a variety of fluid motions that are prescribed by (31b) which exhibit disparate qualitative features for various values of the parameters A and γ_1 .

4.1 Lower fluid layer

Passing to the moving frame by way of the coordinate transformation

$$X(t) = kx(t) - \omega t \quad \text{and} \quad Y(t) = k(y(t) + h), \quad (32)$$

the system is transformed to a nonlinear autonomous dynamical system

$$\begin{cases} \dot{X} = M \cosh Y \cos X - \omega \\ \dot{Y} = M \sinh Y \sin X, \end{cases} \quad (33)$$

where

$$M := \frac{ak\omega}{\sinh(kh)} = \frac{a}{h} \cdot \frac{kh}{\sinh(kh)} \cdot \omega \ll \omega, \quad (34)$$

since $\omega > 0$ by assumption, and $s < \sinh(s)$ for $s > 0$ and $a/h = \mathcal{O}(\epsilon) \ll 1$ in the linear wave regime. The autonomous system (33) meets standard regularity assumptions for the uniqueness of the Cauchy problem [26], therefore its trajectories do not intersect. We note that (33) matches the dynamical system for the lower layer in the irrotational two-layer problem that was studied in [20], and the analysis of the phase portrait is identical. We include here the salient points for completeness. The dynamical system (33) has the standard (canonical) form [26] of Hamilton's equations

$$\dot{X} = \frac{\partial H}{\partial Y}, \quad \dot{Y} = -\frac{\partial H}{\partial X}$$

for the Hamiltonian function $H(X, Y) = M \sinh Y \cos X - \omega Y$ (where we reuse the H notation for convenience: this is not the same as the Hamiltonian functional defined in (15)). Hence, if $(X(t), Y(t))$ is a trajectory of (33), then we have $\frac{d}{dt}H(X(t), Y(t)) = \frac{\partial H}{\partial X}\dot{X} + \frac{\partial H}{\partial Y}\dot{Y} = -\dot{Y}\dot{X} + \dot{X}\dot{Y} = 0$, and so singular points of (33) correspond to critical points of H . The nature of these points can be determined from the Hessian of H , and the associated Morse index, which corresponds to the number of negative eigenvalues of the Hessian. Morse's Lemma [27] implies that points with Morse index 1 are saddle points, whereas centres have Morse indices 0 and 2.

The coordinate transformation (32), together with the periodicity of the dynamical system with respect to X , mean that it suffices to consider $\{X : -\pi \leq X \leq \pi\}$ and $\{Y : 0 \leq Y \leq kh + \epsilon \cos X\}$, where $\epsilon = ak$ is the wave steepness parameter for the internal wave. The 0-isocline is defined to be the set where $dY/dt = 0$, and the ∞ -isocline is the set where $dX/dt = 0$. Therefore the 0-isocline is given by the lines $X = 0, \pm\pi$, and the line segment $Y = 0$. The ∞ -isocline is given in the region $X \in (-\frac{\pi}{2}, \frac{\pi}{2})$ by the curve $(X, \alpha(X))$, where $\alpha(X) \in [Y^*, \infty)$ for $\cosh(Y^*) = \omega/M$, and α is defined as follows: on $[0, \frac{\pi}{2})$ we set α to be the inverse of the function $Y \mapsto \arccos\left(\frac{\omega}{M \cosh(Y)}\right)$ defined on $[Y^*, \infty)$, and extend it by mirror symmetry to the interval $(-\frac{\pi}{2}, \frac{\pi}{2})$. Since $\frac{\omega}{M \cosh(Y)} \leq 1$ for $Y \geq Y^*$, it follows that α is well-defined; furthermore the even function α is smooth, it takes on its infimum Y^* at $X = 0$, and satisfies the limiting condition $\lim_{X \rightarrow \pm\frac{\pi}{2}} \alpha(X) = \infty$. The only singular point of the dynamical system (33), for positive Y , is $Q = (0, Y^*)$, and the Hessian of H at Q is

$$\begin{pmatrix} -M \sinh(Y^*) & 0 \\ 0 & M \sinh(Y^*) \end{pmatrix},$$

and so Morse's Lemma implies that Q is a saddle point. A phase portrait of the dynamical system is given in Figure 3.

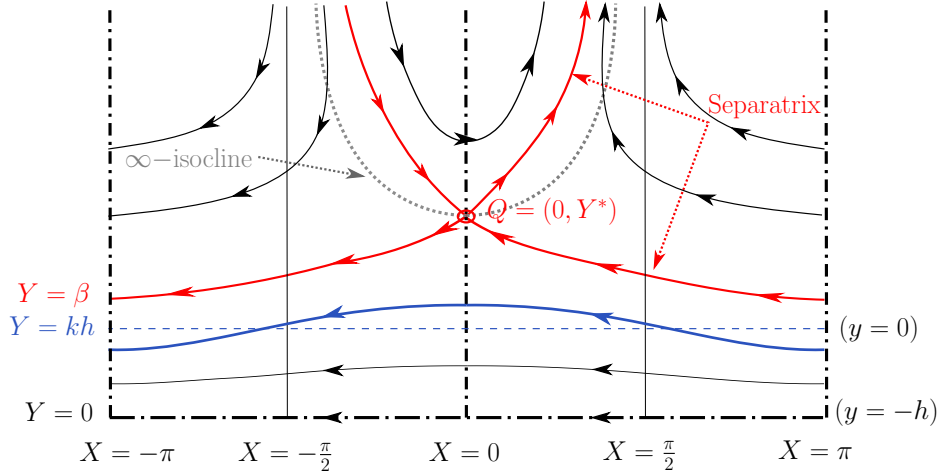


Figure 3: Phase portrait for the lower-fluid layer. The dotted grey line represents the ∞ -isocline, with the dotted-dashed lines --- representing the 0-isoclines. The internal wave profile (—) with mean-water level $Y = kh$ (corresponding to $y = 0$) is also illustrated.

4.2 Upper fluid layer

When considering the fluid motion in the upper layer it is expedient to introduce the change of variables

$$X(t) = kx(t) - \omega t \quad \text{and} \quad Y_1(t) = k(h_1 - y(t)), \quad (35)$$

with these new coordinates transforming the horizontal variable to the moving frame, and reversing the orientation of the vertical coordinates. The system (31b) is thus transformed to the nonlinear autonomous dynamical system

$$\begin{cases} \dot{X} = F(X, Y_1) := M_1 \cos X f(Y_1) - k\mathfrak{c} - \gamma_1 Y_1, \\ \dot{Y}_1 = G(X, Y_1) := M_1 \sin X g(Y_1), \end{cases} \quad (36)$$

where

$$M_1 = a_1 k^2 \mathfrak{c} = \mathfrak{e}_1 k \mathfrak{c}, \quad (37)$$

with $|M_1| = |\mathfrak{e}_1 k \mathfrak{c}| \ll k|\mathfrak{c}|$ (noting that $\mathfrak{e}_1 = a_1 k \ll 1$) and

$$f(Y_1) := A \cosh Y_1 - \sinh Y_1, \quad g(Y_1) := A \sinh Y_1 - \cosh Y_1.$$

For the remainder of the Section we assume that $a_1 > 0$, without loss of generality, since shifting X by $\frac{\pi}{2}$ maps (36) to an identical system with $-a_1$

in place of a_1 . The dynamical system (36) is periodic in X , so we may restrict our attention to the interval $X \in [-\pi, \pi]$. Since the coordinate transformation (35) reverses the vertical orientation, the streamline for the internal wave, $kh_1 - \epsilon \cos X$ will lie above that of the surface wave, $-\epsilon_1 \cos X$, in terms of (X, Y_1) -coordinates, and the upper fluid layer is located in the region $\{Y_1 : -\epsilon_1 \cos X \leq Y_1 \leq kh_1 - \epsilon \cos X\}$. As \dot{X} and \dot{Y}_1 are given by even and odd expressions in X , respectively, via (36), it follows that the corresponding trajectories (along with the 0- and ∞ -isoclines) will be symmetric with respect to the Y_1 axis. It follows immediately from (36) that the points

$$P_{\pm}^{\infty} = \left(\pm \frac{\pi}{2}, -\frac{k\epsilon}{\gamma_1} \right) \quad (38)$$

lie in the ∞ -isocline for any configuration of the system (36). If $\gamma_1 \geq 0$ and $\epsilon > 0$ (and so there is no critical layer) then the points P_{\pm}^{∞} must always lie below the upper fluid domain (in terms of (X, Y_1) -coordinates), while for $\gamma_1 < 0$ the points P_{\pm}^{∞} lie above the upper fluid domain (in terms of (X, Y_1) -coordinates) if $c/|\gamma_1| > h_1$. The dynamical system (36) is also a Hamiltonian system, with Hamiltonian function $H_1(X, Y_1) = M_1 \cos X g(Y_1) - \frac{\gamma_1}{2} Y_1^2 - k\epsilon Y_1$ since

$$\dot{X} = F(X, Y_1) = \frac{\partial H_1}{\partial Y_1}, \quad \dot{Y}_1 = G(X, Y_1) = -\frac{\partial H_1}{\partial X},$$

where H_1 is constant along trajectories of (36), and singular points of (36) correspond to critical points of $H_1(X, Y_1)$. The Hessian matrix of H_1 is

$$D^2 H_1(X, Y_1) = \begin{pmatrix} -M_1 \cos X g(Y_1) & -M_1 \sin X f(Y_1) \\ -M_1 \sin X f(Y_1) & M_1 \cos X g(Y_1) - \gamma_1 \end{pmatrix}. \quad (39)$$

4.3 The case $A = 1$

When $A = 1$, (36) reduces to

$$\begin{cases} \dot{X} = F(X, Y_1) = M_1 \cos X e^{-Y_1} - k\epsilon - \gamma_1 Y_1 \\ \dot{Y}_1 = G(X, Y_1) = -M_1 \sin X e^{-Y_1}. \end{cases} \quad (40)$$

The 0-isocline for (40) (the set where $\dot{Y}_1 = G(X, Y_1) = 0$) consists of the lines $X = 0, \pm\pi$. For $\epsilon > 0$ we have $\dot{Y}_1 < 0$ for $\{X : 0 < X < \pi\}$, while $\dot{Y}_1 > 0$ for $\{X : 0 < X < \pi\}$ when $\epsilon < 0$ (in which case a critical layer also occurs). The ∞ -isocline is defined to be the set of (X, Y_1) for which

$$\dot{X} = F(X, Y_1) = 0 \iff \frac{k\epsilon}{\gamma_1} + Y_1 = \frac{M_1 \cos X e^{-Y_1}}{\gamma_1}. \quad (41)$$

Furthermore, for $A = 1$ expression (22) becomes

$$\frac{a}{a_1} \frac{c}{\mathfrak{c}} = e^{-kh_1} \iff \gamma_1 = \frac{c}{h_1} \left(1 - \frac{a}{a_1} e^{kh_1} \right) \iff M_1 e^{-kh_1} = \omega \mathfrak{e}. \quad (42)$$

From (42) we can immediately infer a number of features of coupled surface and internal waves. For instance, $a_1 \geq a e^{kh_1} \Leftrightarrow \gamma_1 \geq 0$. Furthermore out-of-phase waves only occur if $\frac{c}{\mathfrak{c}} < 0$, which implies that the vorticity $\gamma_1 > 0$ is positive, and a critical layer occurs. In the shallow-water (or long-wave) regime, $kh_1 \ll 1$ and $e^{-kh_1} \approx 1$.

Before constructing some phase portraits of (40), we recall that the Lambert W function is defined [12] to be the inverse of the function xe^x , that is, $W(xe^x) = x$. It is a multivalued function: if $b > 0$, then the equation $xe^x = b$ has one solution given by $x = W(b)$, with $W(\cdot)$ standing for the principal branch of the Lambert W function. When $b \in [-\frac{1}{e}, 0)$, there are two solutions, x_1, x_2 , with $x_1 = W(b)$ and $x_2 = W_{-1}(b)$, with W_{-1} being the second real-valued branch of the Lambert W function. The function $W : [-\frac{1}{e}, \infty) \rightarrow [-1, \infty)$ is increasing in its domain, whereas $W_{-1} : [-\frac{1}{e}, 0) \rightarrow (-\infty, -1]$ is decreasing. Also, $W(-\frac{1}{e}) = W_{-1}(-\frac{1}{e}) = -1$. In summary, we have

$$xe^x = b \iff x = \begin{cases} W(b), & b \geq 0 \\ W(b) \text{ or } W_{-1}(b), & b \in [-\frac{1}{e}, 0). \end{cases} \quad (43)$$

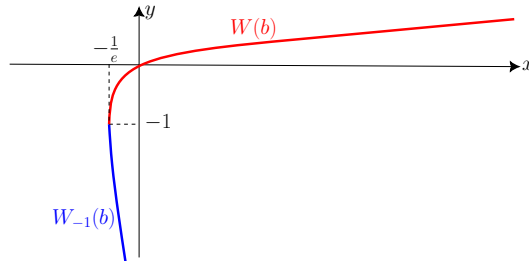


Figure 4: The two real-valued branches of the Lambert W function.

4.3.1 $A = 1$ and $\mathfrak{c} > 0$ (no critical layers)

Proposition 4.1. *For $A = 1$, let $\gamma_1 > 0$ be such that $\mathfrak{c} > 0$. Then the ∞ -isocline of the dynamical system (36) for $X \in [0, \frac{\pi}{2}]$ is given by the graph of a decreasing function of X , and there exists a saddle point located at $Q_0^s = \left(0, W \left(\frac{M_1}{\gamma_1} e^{\frac{k\mathfrak{c}}{\gamma_1}} \right) - \frac{k\mathfrak{c}}{\gamma_1} \right)$, where $W \left(\frac{M_1}{\gamma_1} e^{\frac{k\mathfrak{c}}{\gamma_1}} \right) - \frac{k\mathfrak{c}}{\gamma_1} < 0$. In addition, $\dot{X} < 0$ holds for streamlines lying above the horizontal line $Y_1 = W \left(\frac{M_1}{\gamma_1} e^{\frac{k\mathfrak{c}}{\gamma_1}} \right) - \frac{k\mathfrak{c}}{\gamma_1}$.*

Furthermore, if the condition

$$\mathfrak{e}_1 \frac{\omega}{\gamma_1} e^{\frac{\omega}{\gamma_1}} < e^{-1} \quad (44)$$

holds true, then the ∞ -isocline of the dynamical system (36) in $(\frac{\pi}{2}, \pi]$ consists of the graphs of a decreasing and an increasing function of X . In particular, there exist 2 additional singular points Q^c_π, Q^s_π lying on the vertical line $X = \pi$ which correspond to a centre, and a saddle, respectively. Moreover, $\dot{X} > 0$ for (X, Y_1) between these two graphs.

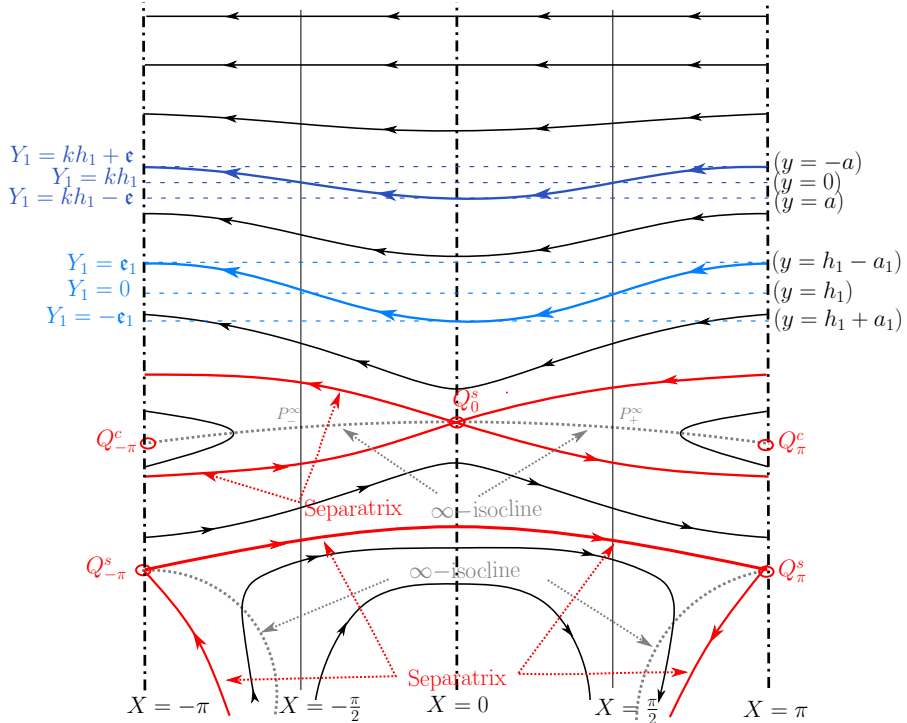


Figure 5: Phase portrait for $A = 1, \gamma_1 > 0, \mathfrak{c} > 0$, and where (44) holds. The dotted grey lines represent the ∞ -isoclines, while the dotted-dashed lines - - - represent the 0 -isoclines. The surface wave profile (—) has mean-water level $Y_1 = 0$, corresponding to $y = h_1$. The internal wave profile (—) has mean water level $Y = kh_1$, corresponding to $y = 0$. Note that the streamline representing the surface wave lies *beneath* that of the internal wave in terms of the (X, Y_1) -coordinates used for this phase portrait.

Proof. First observe that for $\gamma_1 > 0$ and $\mathfrak{c} > 0$, (42) implies that $0 < a < a_1$, and so the surface wave must be larger than the internal wave in this regime.

For $X \in [0, \frac{\pi}{2}]$, where $\cos X \geq 0$, we observe that the condition (41) can be expressed in terms of the Lambert W function (43) as

$$F(X, Y_1) = 0 \iff \frac{k\mathfrak{c}}{\gamma_1} + Y_1 = W\left(e^{\frac{k\mathfrak{c}}{\gamma_1}} \frac{M_1 \cos X}{\gamma_1}\right).$$

Hence the dynamical system (40) has a singular point at $Q_0^s = (0, \bar{Y}_1(0))$, where $\bar{Y}_1(0) = W\left(\frac{M_1}{\gamma_1} e^{\frac{k\mathfrak{c}}{\gamma_1}}\right) - \frac{k\mathfrak{c}}{\gamma_1} < 0$, since $M_1 = \mathfrak{e}_1 k \mathfrak{c} \ll k \mathfrak{c}$ and W is an increasing function on the positive real-line. This non-hyperbolic singular point can be characterised by exploiting the Hamiltonian structure of (36) and Morse theory. The Hessian at Q_0^s is

$$D^2 H_1(0, \bar{Y}_1(0)) = \begin{pmatrix} M_1 e^{-\bar{Y}_1(0)} & 0 \\ 0 & -M_1 e^{-\bar{Y}_1(0)} - \gamma_1 \end{pmatrix},$$

and the diagonal terms have opposite signs, hence Q_0^s is a saddle point lying on the intersection of four separatrices, which are the subsets of the phase space (X, Y_1) for which $H_1(X, Y_1) = H_1(0, \bar{Y}_1(0))$. We note that $F(X, 0) = M_1 \cos X - k\mathfrak{c} = \mathfrak{e}_1 k \mathfrak{c} \cos X - k\mathfrak{c} < 0$, due to (37), and $F(X, kh_1) = M_1 \cos X e^{-kh_1} - \omega = \mathfrak{e}\omega \cos X - \omega < 0$, due to (34) and (42).

To establish the second claim, if the assumed condition (44) on the wave-steepness holds then $-\frac{1}{e} < \frac{M_1 \cos X}{\gamma_1} e^{\frac{k\mathfrak{c}}{\gamma_1}} < 0$ when $X \in (\frac{\pi}{2}, \pi]$. The ∞ -isocline then consists of two different sets of points $(X, \bar{Y}_1(X))$ and $(X, Y_1^*(X))$ which are formed by the respective branches of the Lambert W function (43), namely:

$$\bar{Y}_1(X) = W\left(\frac{M_1 \cos X}{\gamma_1} e^{\frac{k\mathfrak{c}}{\gamma_1}}\right) - \frac{k\mathfrak{c}}{\gamma_1}, \quad Y_1^*(X) = W_{-1}\left(\frac{M_1 \cos X}{\gamma_1} e^{\frac{k\mathfrak{c}}{\gamma_1}}\right) - \frac{k\mathfrak{c}}{\gamma_1}.$$

The monotonicity properties of the Lambert W function, and the fact that $X \in (\frac{\pi}{2}, \pi]$, together yield that the former branch corresponds to the graph of a decreasing function, and the latter to that of an increasing one. Recalling the form of the 0 -isocline, there are singular points $Q_\pi^c = (\pi, \bar{Y}_1(\pi))$ and $Q_\pi^s = (\pi, Y_1^*(\pi))$ where

$$\bar{Y}_1(\pi) = W\left(-\frac{M_1}{\gamma_1} e^{\frac{k\mathfrak{c}}{\gamma_1}}\right) - \frac{k\mathfrak{c}}{\gamma_1} \quad \text{and} \quad Y_1^*(\pi) = W_{-1}\left(-\frac{M_1}{\gamma_1} e^{\frac{k\mathfrak{c}}{\gamma_1}}\right) - \frac{k\mathfrak{c}}{\gamma_1}.$$

For the point Q_π^c the Hessian is

$$D^2 H_1(\pi, \bar{Y}_1(\pi)) = \begin{pmatrix} -M_1 e^{-\bar{Y}_1(\pi)} & 0 \\ 0 & M_1 e^{-\bar{Y}_1(\pi)} - \gamma_1 \end{pmatrix},$$

while the Hessian at Q_π^s is given by

$$D^2 H_1(\pi, Y_1^*(\pi)) = \begin{pmatrix} -M_1 e^{-Y_1^*(\pi)} & 0 \\ 0 & M_1 e^{-Y_1^*(\pi)} - \gamma_1 \end{pmatrix}.$$

For fixed $X \in (-\frac{\pi}{2}, \pi]$, $F(X, \cdot)$ is increasing for $Y_1 < \ln\left(-\frac{M_1 \cos X}{\gamma_1}\right)$, and decreasing for Y_1 above this value. Note that $\ln\left(-\frac{M_1 \cos X}{\gamma_1}\right) < -1 - \frac{k\mathfrak{c}}{\gamma_1} < -\mathfrak{e}_1$, since we are assuming that $\frac{M_1}{\gamma_1} e^{\frac{k\mathfrak{c}}{\gamma_1}} < \frac{1}{e}$. These monotonicity properties imply that

$$M_1 e^{-\bar{Y}_1(\pi)} - \gamma_1 = \frac{\partial F}{\partial Y_1}(\pi, \bar{Y}_1(\pi)) < 0, \quad M_1 e^{-Y_1^*(\pi)} - \gamma_1 = \frac{\partial F}{\partial Y_1}(\pi, Y_1^*(\pi)) > 0.$$

Since $M_1 > 0$, Morse theory implies that $Q_\pi^c = (\pi, \bar{Y}_1(\pi))$ corresponds to a centre, as it has Morse index 2, and $Q_\pi^s = (\pi, Y_1^*(\pi))$ to a saddle, as it has Morse index 1. Finally, the fact that $F(X, \cdot)$ changes monotonicity once in Y_1 , for fixed X , first being increasing, shows that $\dot{X} > 0$ between the two branches of the ∞ -isocline. \square

Remark 4.1. *In order for all singular points for the dynamical system (36) considered in Proposition 4.1 to lie below the fluid domain we need*

$$W\left(\frac{M_1}{\gamma_1} e^{\frac{k\mathfrak{c}}{\gamma_1}}\right) - \frac{k\mathfrak{c}}{\gamma_1} = W\left(\frac{\mathfrak{e}\omega}{\gamma_1} e^{\frac{\omega}{\gamma_1}}\right) - \frac{\omega}{\gamma_1} + kh_1 < -\mathfrak{e}_1.$$

If this holds true, then $\dot{X} < 0$ along all streamlines.

Remark 4.2. *Two saddle-centre bifurcations occur when $\frac{M_1}{\gamma_1} e^{\frac{k\mathfrak{c}}{\gamma_1}}$ crosses the value $-\frac{1}{e}$: there is a transition from 1 to 5 critical points for the dynamical system.*

Proposition 4.2. *For $A = 1$, let $\gamma_1 < 0$ (and so $\mathfrak{c} > 0$). Then the ∞ -isocline of the dynamical system (36) in $[\frac{\pi}{2}, \pi]$ is given by the graph of an increasing function of X , and there exists a saddle point located at $Q_\pi^s = \left(\pi, W\left(-\frac{M_1}{\gamma_1} e^{\frac{k\mathfrak{c}}{\gamma_1}}\right) - \frac{k\mathfrak{c}}{\gamma_1}\right)$, where $W\left(-\frac{M_1}{\gamma_1} e^{\frac{k\mathfrak{c}}{\gamma_1}}\right) - \frac{k\mathfrak{c}}{\gamma_1} > 0$. In addition, $\dot{X} > 0$ for (X, Y_1) above this graph. Furthermore, if the condition*

$$\mathfrak{e}_1 e^{\mathfrak{e}_1} < 1 \tag{45}$$

holds true, then the ∞ -isocline for the dynamical system (36) in $[0, \frac{\pi}{2}]$ consists of the graphs of a decreasing and an increasing function of X . In particular, there exist 2 additional singular points Q_0^c, Q_0^s lying on the vertical line $X = 0$ which correspond to a centre, and a saddle, respectively. Moreover, $\dot{X} < 0$ for (X, Y_1) between the two graphs.

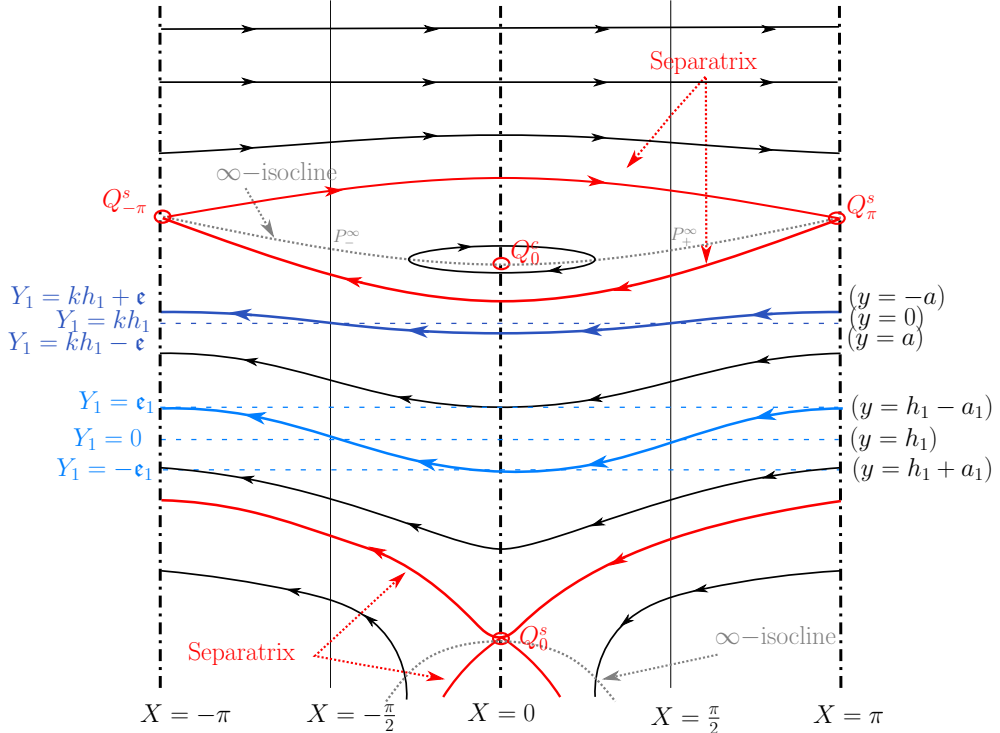


Figure 6: Phase portrait for $A = 1$, $\mathfrak{c} > 0$, $\gamma_1 < 0$, where (45) holds. A similar legend applies as in Figure 5.

Proof. Note that (42) implies that $a > a_1 e^{-kh_1} > 0$ for $\gamma_1 < 0$, and hence the internal and surface waves must be in-phase in this regime. Since many elements of the proof follow that of Proposition 4.1 (upon swapping the intervals $[-\frac{\pi}{2}, \frac{\pi}{2}]$ and $[-\pi, \pi] \setminus [-\frac{\pi}{2}, \frac{\pi}{2}]$) we just provide the essential details. When $X \in [\frac{\pi}{2}, \pi]$, condition (41) prescribing the ∞ -isocline can be reexpressed as

$$F(X, Y_1) = 0 \iff Y_1 = W\left(\frac{M_1 \cos X}{\gamma_1} e^{\frac{k\mathfrak{c}}{\gamma_1}}\right) - \frac{k\mathfrak{c}}{\gamma_1},$$

since $\gamma_1 < 0$. We note that $\frac{\partial F}{\partial Y_1} > 0$ for points along the ∞ -isocline when $X \in [\frac{\pi}{2}, \pi]$. The ∞ -isocline is given by the graph of the increasing function $W\left(\frac{M_1 \cos X}{\gamma_1} e^{\frac{k\mathfrak{c}}{\gamma_1}}\right) - \frac{k\mathfrak{c}}{\gamma_1}$ in this case. Recalling the form of the 0-isocline, there is a singular point at $Q_\pi^s = (\pi, \bar{Y}_1(\pi))$, where $\bar{Y}_1(\pi) = W\left(-\frac{M_1}{\gamma_1} e^{\frac{k\mathfrak{c}}{\gamma_1}}\right) - \frac{k\mathfrak{c}}{\gamma_1} > 0$. The Hessian at Q_π^s is given by

$$D^2H_1(\pi, \bar{Y}_1(\pi)) = \begin{pmatrix} M_1 e^{-\bar{Y}_1(\pi)} & 0 \\ 0 & -M_1 e^{-\bar{Y}_1(\pi)} - \gamma_1 \end{pmatrix}.$$

Since M_1 is positive, and $\frac{\partial F}{\partial Y_1}(\pi, \bar{Y}_1(\pi)) = -M_1 e^{-\bar{Y}_1(\pi)} - \gamma_1 > 0$ due to the monotonicity properties of $F(X, \cdot)$ along the ∞ -isocline for $X \in [\frac{\pi}{2}, \pi]$, this point has Morse index 1 and hence Q_π^s is a saddle.

If (45) holds, note that $\epsilon_1 e^{\epsilon_1} < 1$ implies that $\frac{M_1}{\gamma_1} e^{\frac{k\epsilon}{\gamma_1}} > -\frac{1}{e}$ since

$$\begin{aligned} \epsilon_1 e^{\epsilon_1} < 1 &\implies \frac{M_1}{\gamma_1} e^{\epsilon_1} > \frac{k\epsilon}{\gamma_1} & (46) \\ \implies \frac{M_1}{\gamma_1} e^{\epsilon_1} > \frac{k\epsilon}{\gamma_1} - \epsilon_1 &\implies \frac{M_1}{\gamma_1} e^{\frac{k\epsilon}{\gamma_1}} > \left(\frac{k\epsilon}{\gamma_1} - \epsilon_1\right) e^{\frac{k\epsilon}{\gamma_1} - \epsilon_1} > -\frac{1}{e}, \end{aligned}$$

where $M_1 = \epsilon_1 k \epsilon$ and the last step follows from observing that the function se^s has a minimum value at $s = -1$. Thus, since $X \in [0, \frac{\pi}{2})$, relation (43) implies that the equation $F(X, Y_1) = 0$ has two solutions in Y_1 , for fixed X in this range, and so the ∞ -isocline consists of the graphs of the functions

$$\bar{Y}_1(X) = W\left(\frac{M_1 \cos X}{\gamma_1} e^{\frac{k\epsilon}{\gamma_1}}\right) - \frac{k\epsilon}{\gamma_1} \quad \text{and} \quad Y_1^*(X) = W_{-1}\left(\frac{M_1 \cos X}{\gamma_1} e^{\frac{k\epsilon}{\gamma_1}}\right) - \frac{k\epsilon}{\gamma_1}.$$

Recalling that the 0 -isocline consists of the lines $\{X = 0, \pm\pi\}$, there exist additional singular points $Q_0^s = (0, Y_1^*(0))$, $Q_0^c = (0, \bar{Y}_1(0))$, where

$$\bar{Y}_1(0) = W\left(\frac{M_1}{\gamma_1} e^{\frac{k\epsilon}{\gamma_1}}\right) - \frac{k\epsilon}{\gamma_1} > 0, \quad Y_1^*(0) = W_{-1}\left(\frac{M_1}{\gamma_1} e^{\frac{k\epsilon}{\gamma_1}}\right) - \frac{k\epsilon}{\gamma_1} < 0.$$

Since $M_1 > 0$, evaluating the Hessian $D^2 H_1$ (39) implies by Morse theory that $Q_0^c = (0, \bar{Y}_1(0))$ corresponds to a centre, since $\frac{\partial F}{\partial Y_1}(0, \bar{Y}_1(0)) > 0$, whereas $(0, Y_1^*(0))$ is a saddle point since $\frac{\partial F}{\partial Y_1}(0, Y_1^*(0)) < 0$. \square

Remark 4.3. *In order for all singular points for the dynamical system (36) considered in Proposition 4.2 to lie outside the fluid domain we require*

$$\epsilon < W\left(\frac{\epsilon\omega}{\gamma_1} e^{\frac{\omega}{\gamma_1}}\right) - \frac{\omega}{\gamma_1}$$

in order to ensure that Q_π^s lies above $Y_1 = kh_1 + \epsilon$. Note that it follows from the monotonicity of W_{-1} , and (46), that Q_0^s will lie below $Y_1 = \epsilon_1$ since $W_{-1}\left(\frac{M_1}{\gamma_1} e^{\frac{k\epsilon}{\gamma_1}}\right) < \frac{k\epsilon}{\gamma_1} - \epsilon_1$. Also $\dot{X} < 0$ along all streamlines in the upper fluid layer.

4.3.2 $A = 1$ and $\epsilon < 0$ (critical layer present)

Proposition 4.3. *For $A = 1$, let $\gamma_1 > 0$ be such that $\epsilon < 0$. The ∞ -isocline for the dynamical system (36) in $[\frac{\pi}{2}, \pi]$ is given by the graph of an increasing*

function of X , and there exists a saddle point located at $Q_\pi^s = \left(\pi, W\left(-\frac{M_1}{\gamma_1}e^{\frac{kc}{\gamma_1}}\right) - \frac{kc}{\gamma_1}\right)$. In addition, $\dot{X} < 0$ along streamlines lying above the horizontal line $Y_1 = W\left(-\frac{M_1}{\gamma_1}e^{\frac{kc}{\gamma_1}}\right) - \frac{kc}{\gamma_1}$. Furthermore, if the condition

$$c_1 e^{c_1} < 1 \quad (47)$$

holds true, then the ∞ -isocline for the dynamical system (36) in $[0, \frac{\pi}{2}]$ consists of the graphs of a decreasing and an increasing function of X . In particular, there exist 2 additional singular points, Q_0^s, Q_0^c , corresponding to a saddle point and a centre respectively, lying at the vertical line $X = 0$. Moreover, $\dot{X} > 0$ for (X, Y_1) between the two graphs.

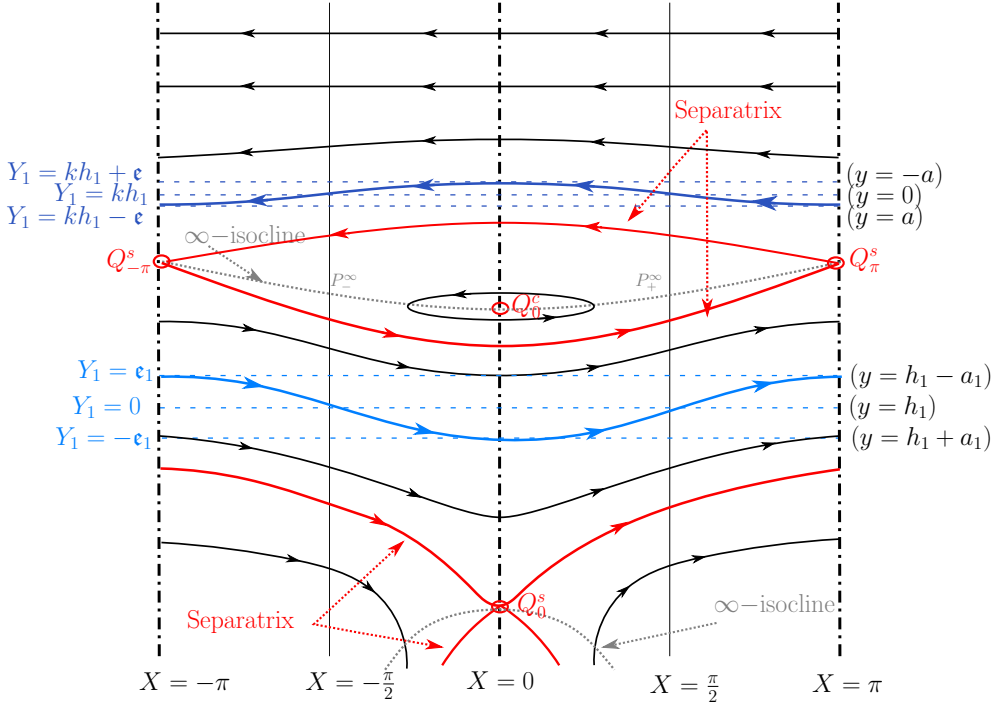


Figure 7: Phase portrait for $A = 1$, $c < 0$ ($\gamma_1 > 0$), where (47) holds. A similar legend applies as in Figure 5.

Proof. For $c < 0$, it follows from (42) that $a/a_1 < 0$, and hence the internal and surface waves must be out of phase. Noting that the relation (41), which defines the ∞ -isocline, features the parameters c and γ_1 solely by

way of their ratio. Therefore swapping the signs of each of these terms does not materially affect the considerations of Proposition 4.2 relating to the structure of the ∞ -isocline, and the existence and location of singular points. When $\cos X < 0$, $\frac{\partial F}{\partial Y_1}(X, \cdot) < 0$; when $\cos X > 0$, $F(X, \cdot)$ is increasing for $Y_1 < \ln\left(-\frac{M_1 \cos X}{\gamma_1}\right)$, while $F(X, \cdot)$ is decreasing for Y_1 above this value. Using similar reasoning to Propositions 4.1 and 4.2, determining the sign of the eigenvalues for the Hessian (39) we deduce that $Q_0^s = (0, Y_1^*(0))$ corresponds to a saddle point, since $\frac{\partial F}{\partial Y_1}(0, Y_1^*(0)) > 0$ and $M_1 < 0$; $Q_0^c = (0, \bar{Y}_1(0))$ must be a centre, since $\frac{\partial F}{\partial Y_1}(0, \bar{Y}_1(0)) < 0$; while $Q_{\pm\pi}^s = (\pm\pi, \bar{Y}_1(\pi))$ correspond to saddle points, since $\frac{\partial F}{\partial Y_1}(\pm\pi, \bar{Y}_1(\pi)) < 0$, also recalling the sign of M_1 .

For $\mathfrak{c} < 0$, the points $P_{\pm}^{\infty} = \left(\pm\frac{\pi}{2}, -\frac{k\mathfrak{c}}{\gamma_1}\right)$ from the ∞ -isocline must be located within the fluid domain, by inspection. When condition (47) holds, the saddle point $Q_0^s = (0, Y_1^*(0))$ lies outside the fluid domain (beneath the surface wave in terms of (X, Y_1) -coordinates). Then the branches of the separatrices which join the points $Q_{\pm\pi}^s$ represent critical layers for fluid motion in the upper layer, demarcating a vortex centred at Q_0^c which has streamlines redolent of the Kelvin's cat's eyes patterns observed in the single fluid layer model [3]. We infer from inspecting $\frac{\partial F}{\partial Y_1}$ that $\dot{X} > 0$ for streamlines in the fluid domain which lie under the upper ∞ -isocline, while $\dot{X} < 0$ for streamlines in the fluid domain which lie above the upper ∞ -isocline.

□

Remark 4.4. Suppose that (47) holds, then in order for the critical layer to be located in the fluid domain the inequalities

$$\frac{\omega}{\gamma_1} < W\left(\frac{\mathfrak{e}\omega}{\gamma_1} e^{\frac{\omega}{\gamma_1}}\right) + kh_1 \quad \text{and} \quad W\left(-\frac{\mathfrak{e}\omega}{\gamma_1} e^{\frac{\omega}{\gamma_1}}\right) < \frac{\omega}{\gamma_1} - \mathfrak{e},$$

must hold, which offers a further condition on \mathfrak{e} .

4.4 The case $A < 1$

As observed in Lemma 3.1, A is permitted to be negative for rotational flows (with a lower bound of $A \geq -\gamma_1^2/4gk$), which adds an additional level of complexity compared to the setting of purely irrotational fluid layers considered in [20, 21]. From (27) we observe that

$$e^{-kh_1} < \frac{a}{a_1} \frac{c}{\mathfrak{c}} < \mathfrak{U}, \quad (48)$$

where $\mathfrak{U} = \cosh kh_1 + \gamma_1^2 \sinh kh_1/4gk$. As stated previously, we assume without loss of generality that $a_1, c > 0$ in subsequent considerations. Hence,

(48) implies that waves are in phase ($a/a_1 > 0$) if and only if $\mathfrak{c} > 0$ ($M_1 > 0$). Hence, $\mathfrak{c} < 0$ ($M_1 < 0$) implies both the existence of a critical layer, and out-of-phase waves, as we might expect from the considerations of Section 4.3. In addition, when $\mathfrak{c} > 0$, (48) implies that:

$$\frac{c}{h_1} \left(1 - \frac{a}{a_1} e^{kh_1} \right) < \gamma_1 < \frac{c}{h_1} \left(1 - \frac{a}{a_1} \frac{1}{\mathfrak{U}} \right),$$

with $\mathfrak{c} < 0$ yielding the reverse inequality. In particular, if $\mathfrak{c} > 0$ then $a < a_1 \mathfrak{U}$ for $\gamma_1 > 0$, while $a_1 < ae^{kh_1}$ for $\gamma_1 < 0$, whereas for $\mathfrak{c} < 0$ (and so $\gamma_1 > 0$) then $a_1 > ae^{kh_1}$.

For the remainder of this section we assume that $|A| < 1$ (the condition $\gamma_1^2 \leq 4gk$ is sufficient for this to hold). Regarding the dynamical system (36), in this setting we have $g(Y_1) = A \sinh Y_1 - \cosh Y_1 < 0$ for all $Y_1 \in \mathbb{R}$. Therefore, when $\mathfrak{c} > 0$, $\dot{Y}_1 > 0$ for $X \in (-\pi, 0)$ and $\dot{Y}_1 < 0$ for $X \in (0, \pi)$, with the inequality signs reversed for $\mathfrak{c} < 0$. The 0 –isocline must consist solely of the lines $\{X = 0, \pm\pi\}$. The ∞ –isocline for (36) consists of the set of points for which the function $F(X, Y_1) = 0$, and in order to determine the form of the ∞ –isocline a detailed insight into the monotonicity properties of $F(X, \cdot)$ is required, with

$$\frac{\partial F}{\partial Y_1} = M_1 \cos X g(Y_1) - \gamma_1. \quad (49)$$

For $|A| < 1$ we also have $\frac{\partial^3 F}{\partial Y_1^3}(X, Y_1) < 0$ when $X \in (-\frac{\pi}{2}, \frac{\pi}{2})$, and $\frac{\partial^3 F}{\partial Y_1^3}(X, Y_1) > 0$ when $X \in [-\pi, \pi] \setminus [-\frac{\pi}{2}, \frac{\pi}{2}]$, for all Y_1 . Also $\frac{\partial^2 F}{\partial Y_1^2}(\pm\frac{\pi}{2}, Y_1) = 0$ for all Y_1 . For $|A| < 1$ the quantity $\mathcal{A} := \frac{1+A}{1-A}$ is well-defined, and $f(\mathcal{A}) = 0$. The relation $\frac{\partial^2 F}{\partial Y_1^2}(X, \frac{1}{2} \ln(\frac{1+A}{1-A})) = 0$ then holds true for all $X \in [-\pi, \pi]$.

4.4.1 $|A| < 1$ and $\mathfrak{c} > 0$ (no critical layers)

For $\mathfrak{c} > 0$ (and so $M_1 > 0$) the vorticity must satisfy either $0 < \gamma_1 < \frac{c}{h_1}$, or $\gamma_1 < 0$. If $0 < \gamma_1 < \frac{c}{h_1}$ and $X \in [-\frac{\pi}{2}, \frac{\pi}{2}]$, then (49) implies that $\frac{\partial F}{\partial Y_1} < 0$, and hence the ∞ –isocline is not empty by the implicit function theorem. Analogously, for $\gamma_1 < 0$ and $X \in [-\pi, \pi] \setminus (-\frac{\pi}{2}, \frac{\pi}{2})$, (49) implies that $\frac{\partial F}{\partial Y_1} > 0$, and again the ∞ –isocline is not empty by the implicit function theorem.

In the case of either $0 < \gamma_1 < \frac{c}{h_1}$ and a fixed $X \in [-\pi, \pi] \setminus [-\frac{\pi}{2}, \frac{\pi}{2}]$, or $\gamma_1 < 0$ and $X \in (-\frac{\pi}{2}, \frac{\pi}{2})$, there is the possibility of $\frac{\partial F}{\partial Y_1}$ having two zeros in Y_1 . For such fixed values of X , we will establish that the monotonicity behaviour of $F(X, \cdot)$ matches either that of the function $\mathcal{F}(Y_1)$ in Figure 8, or its negative.

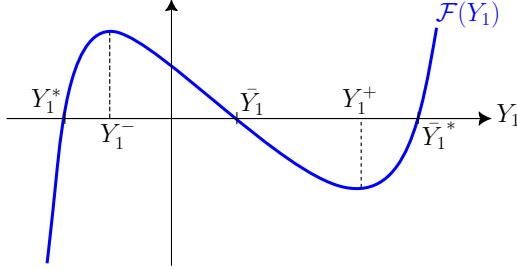


Figure 8: Schematic of the function $\mathcal{F}(Y_1)$, when $A < 1$.

Thus, to determine the structure of the ∞ -isocline, and the existence of singular points for the dynamical system (36), it suffices to estimate the location of maximum and minimum values of $F(X, \cdot)$ for X in the given ranges. Relation (49) implies that

$$\frac{\partial F}{\partial Y_1} = 0 \iff \sqrt{1 - A^2} M_1 \cos X \cosh Y_1^A = -\gamma_1,$$

where $Y_1^A := Y_1 - \frac{1}{2} \ln \mathcal{A}$. Bearing in mind $|A| < 1$, we define

$$\mathfrak{R} := \frac{\sqrt{1 - A^2} M_1}{\gamma_1} \quad \text{and} \quad z_1(X) := \frac{1}{|\mathfrak{R} \cos X|} \quad \text{for } X \neq \frac{\pi}{2}.$$

Then, for $X \neq \frac{\pi}{2}$ and $|\mathfrak{R}| \leq 1$, the local extrema of $F(X, \cdot)$ are

$$\begin{aligned} Y_1^\pm(X) &= \frac{1}{2} \ln \mathcal{A} \pm \operatorname{arcosh} z_1(X) \\ &= \ln \mathcal{A}^{1/2} \pm \ln \left(z_1(X) + \sqrt{z_1^2(X) - 1} \right) \end{aligned} \quad (50)$$

with

$$\begin{aligned} F(X, Y_1^\pm(X)) &= \mp \sqrt{1 - A^2} M_1 \cos X \sinh(\operatorname{arcosh} z_1(X)) - k\mathfrak{c} - \gamma_1 Y_1^\pm(X) \\ &= \gamma_1 \left[\pm (\tanh \operatorname{arcosh} z_1(X) - \operatorname{arcosh} z_1(X)) - \frac{k\mathfrak{c}}{\gamma_1} - \frac{1}{2} \ln \mathcal{A} \right], \\ F(X, Y_1^+(X)) F(X, Y_1^-(X)) &= \gamma_1^2 \left[\left(\frac{k\mathfrak{c}}{\gamma_1} + \frac{1}{2} \ln \mathcal{A} \right)^2 - (\tanh \operatorname{arcosh} z_1(X) - \operatorname{arcosh} z_1(X))^2 \right], \end{aligned}$$

noting that $[\tanh \operatorname{arcosh} x - \operatorname{arcosh} x]' = -\sqrt{x^2 - 1}/x^2$, for $x \geq 1$. Moreover,

$$\begin{aligned} F(X, Y_1^+(X)) F(X, Y_1^-(X)) &< 0 \\ \iff \operatorname{arcosh} z_1(X) - \tanh \operatorname{arcosh} z_1(X) &> \left| \frac{k\mathfrak{c}}{\gamma_1} + \frac{1}{2} \ln \mathcal{A} \right|. \end{aligned}$$

The last inequality allows us to determine the number of possible solutions of the equation $F(X, \cdot) = 0$, for fixed $X \neq \pm \frac{\pi}{2}$, according to the sign of the values of $F(X, \cdot)$ at its critical points. In particular, if

$$\operatorname{arcosh} \frac{1}{|\mathfrak{R}|} - \tanh \operatorname{arcosh} \frac{1}{|\mathfrak{R}|} > \left| \frac{k\mathfrak{c}}{\gamma_1} + \frac{1}{2} \ln \mathcal{A} \right|, \quad (51)$$

then

$$F(X, Y_1^+(X))F(X, Y_1^-(X)) < 0,$$

for all X such that this expression is well defined.

Proposition 4.4. *For $|A| < 1$, let $\gamma_1 > 0$ be such that $\mathfrak{c} > 0$. If $|\mathfrak{R}| < 1$ and (51) holds, then the dynamical system (36) has 7 singular points.*

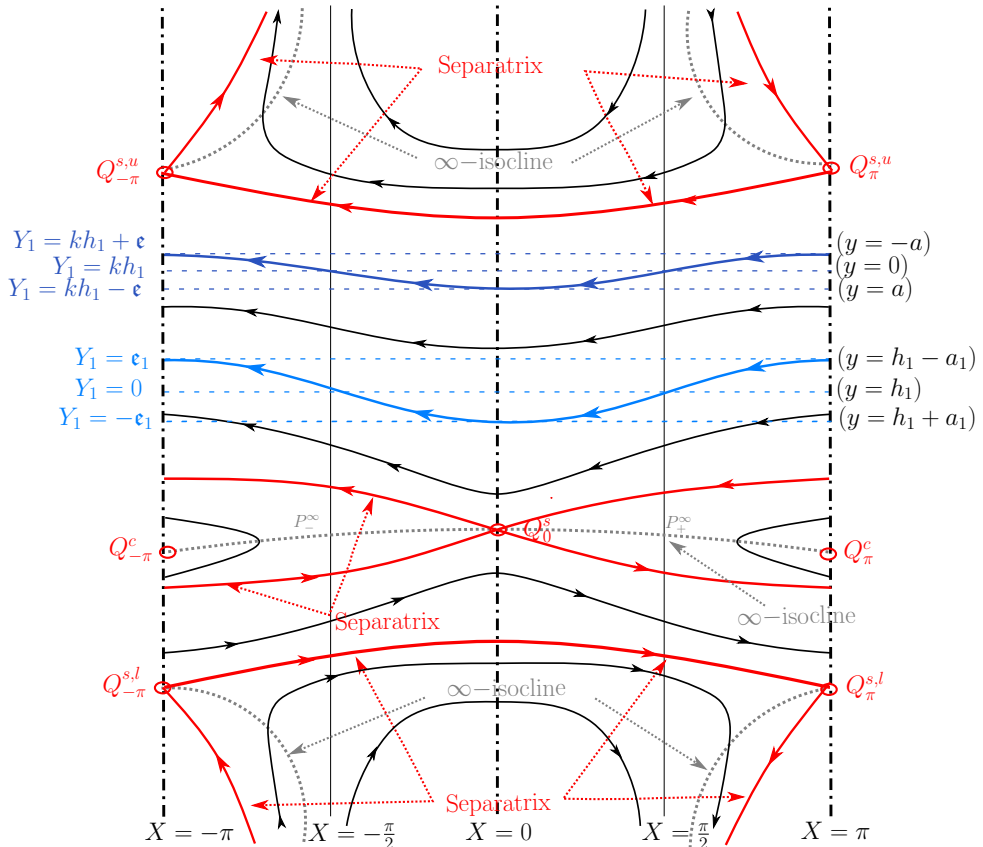


Figure 9: Phase portrait for $A < 1$, $\mathfrak{c} > 0$, $\gamma_1 > 0$, where (51) holds. The dotted grey line represents the ∞ -isocline, while the dotted-dashed lines - - - represent the 0 -isoclines. The surface wave profile (—) has mean-water level $Y_1 = 0$, corresponding to $y = h_1$. The internal wave profile (—) has mean water level $Y = kh_1$, corresponding to $y = 0$.

Proof. From (49)

$$\begin{aligned} \frac{\partial F}{\partial Y_1} &= M_1 \cos X g(Y_1) - \gamma_1 \\ &= -\sqrt{1 - A^2} M_1 \cos X \cosh \left(Y_1 - \frac{1}{2} \ln \mathcal{A} \right) - \gamma_1. \end{aligned} \quad (52)$$

Thus, $F(X, \cdot)$ is decreasing for $|X| \leq \frac{\pi}{2}$, with the ∞ -isocline being non-empty, due to the implicit function theorem, and there exists a singular point along the line $X = 0$, which we label $Q_0^s = (0, \bar{Y}_1(0))$. The analysis in the preceding section allows us to deduce that the equation $F(X, Y_1) = 0$ has three roots in Y_1 , when $\frac{\pi}{2} < |X|$, due to (51): $F(X, \cdot)$ shares similar monotonicity properties as the function $\mathcal{F}(Y_1)$ in Figure 8. We label the singular points as $Q_{\pm\pi}^{s,l} = (\pm\pi, Y_1^*(\pi))$, $Q_{\pm\pi}^c = (\pm\pi, \bar{Y}_1(\pi))$, $Q_{\pm\pi}^{s,u} = (\pm\pi, \bar{Y}_1^*(\pi))$, where the Y_1 coordinates have the ordering $Y_1^*(\pi) < Y_1(\pi) < \bar{Y}_1^*(\pi)$, and will use Morse theory in order to characterise the singular points. At $Q_0^s = (0, \bar{Y}_1(0))$,

$$D^2 H_1(0, \bar{Y}_1(0)) = \begin{pmatrix} -M_1 g(\bar{Y}_1(0)) & 0 \\ 0 & M_1 g(\bar{Y}_1(0)) - \gamma_1 \end{pmatrix},$$

with $-M_1 g(\bar{Y}_1(0)) = M_1 \sqrt{1 - A^2} \cosh(\bar{Y}_1(0) - \frac{1}{2} \ln \mathcal{A}) > 0$, $M_1 g(\bar{Y}_1(0)) - \gamma_1 < 0$, due to the monotonicity conferred by (52). Hence Q_0^s is indeed a saddle point. For the remaining singular points, we need to determine the nature of the eigenvalues of

$$D^2 H_1(\pi, Y_1) = \begin{pmatrix} M_1 g(Y_1) & 0 \\ 0 & -M_1 g(Y_1) - \gamma_1 \end{pmatrix},$$

for Y_1 being $Y_1^*(\pi)$, $\bar{Y}_1(\pi)$, or $\bar{Y}_1^*(\pi)$. In order to do so, we will use the monotonicity properties of $F(\pi, \cdot)$ which match the one for $\mathcal{F}(Y_1)$, in Figure 8. Since $M_1 g(Y_1) < 0$, for any Y_1 , due to $A < 1$ and $M_1 > 0$, it suffices to examine the monotonicity of $F(X, \cdot)$ as it crosses the points $Y_1^*(\pi)$, $\bar{Y}_1(\pi)$ and $\bar{Y}_1^*(\pi)$, in order to conclude about the remaining critical points. Recalling Figure 8 and (39), it follows that $Q_{\pm\pi}^{s,l} = (\pm\pi, Y_1^*(\pi))$ and $Q_{\pm\pi}^{s,u} = (\pm\pi, \bar{Y}_1^*(\pi))$ are saddle points, while $Q_{\pm\pi}^c = (\pm\pi, \bar{Y}_1(\pi))$ is a centre. \square

Remark 4.5. *Physically relevant streamlines must lie between (and avoid) the singular points Q_0^s and $Q_{\pm\pi}^{s,u}$, which provides additional physical conditions for the wave-steepness parameters ϵ, ϵ_1 . Furthermore $\dot{X} < 0$ along any physically relevant streamline in the (X, Y_1) -plane.*

Proposition 4.5. For $|A| < 1$, let $\gamma_1 < 0$ (and so $\mathfrak{c} > 0$) and $|\mathfrak{R}| < 1$. If (51) holds and

$$F\left(X, \frac{1}{2} \ln \mathcal{A}\right) = -k\mathfrak{c} - \frac{\gamma_1}{2} \ln \mathcal{A} \neq 0, \quad (53)$$

then the dynamical system (36) has 5 singular points.

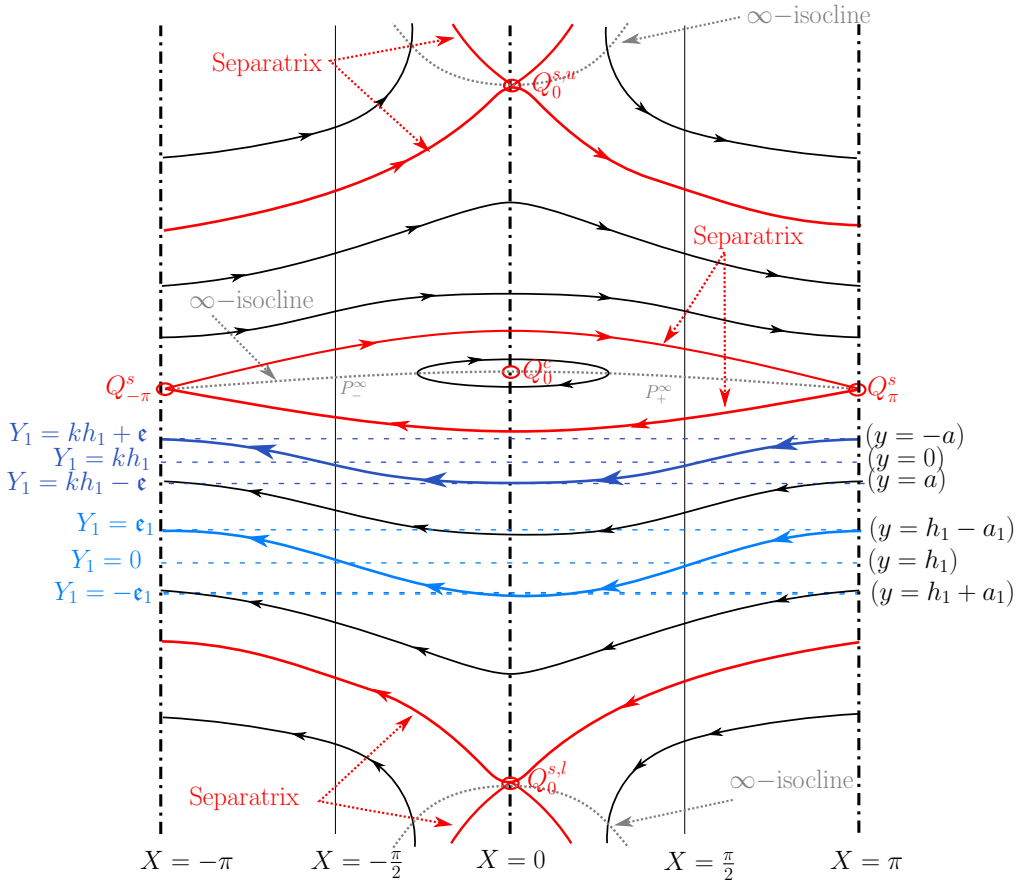


Figure 10: Phase portrait for $A < 1$, $\gamma_1 < 0$ ($\mathfrak{c} > 0$), where (51) holds. The schematic corresponds to a regime whereby $\bar{Y}_1(X) > \frac{1}{2} \ln \mathcal{A}$ for all X . A similar legend applies as in Figure 9.

Proof. The proof of Proposition 4.5 follows along the lines of Proposition 4.4, with some essential differences that we outline briefly. First, $F(X, \cdot)$ shares similar monotonicity properties as $-\mathcal{F}(Y_1)$ of Figure 8 when $\cos X > 0$. Since (51) holds, we infer that the ∞ -isocline comprises the graph of a function $\bar{Y}_1(X)$ which is well-defined for all X . Using the fact that $F(X, \bar{Y}_1(X)) = 0$,

and performing an implicit differentiation, we obtain:

$$\frac{\partial \bar{Y}_1}{\partial X} \frac{\partial F}{\partial Y_1}(X, \bar{Y}_1(X)) = M_1 \sin X f(\bar{Y}_1(X)),$$

for all X in our domain, so that the location of the line $Y_1 = \frac{1}{2} \ln \mathcal{A}$ plays a key role in determining the monotonicity of \bar{Y}_1 . As the monotonicity behaviour of $F(X_0, \cdot)$ matches that of $-\mathcal{F}(Y_1)$ when $\cos X_0 > 0$, and $F(X_0, \cdot)$ is increasing otherwise, it follows that $\frac{\partial F}{\partial Y_1}(X_0, \bar{Y}_1(X_0)) > 0$, for all X_0 . Then, if $\bar{Y}_1(X) < \frac{1}{2} \ln \mathcal{A}$ for all $X \in [-\pi, \pi]$, it follows from examining the sign of f that \bar{Y}_1 is increasing for $X \in (0, \pi)$, and decreasing otherwise. In the case where the relative positions of the horizontal line $Y_1 = \frac{1}{2} \ln \mathcal{A}$ and the graph of \bar{Y}_1 are reversed, a reversal in the monotonicity properties of \bar{Y}_1 also takes place. We note that the graph of \bar{Y}_1 does not intersect the horizontal line $Y_1 = \frac{1}{2} \ln \mathcal{A}$, since $F(X, \frac{1}{2} \ln \mathcal{A}) = -k\mathbf{c} - \frac{\gamma_1}{2} \ln \mathcal{A} \neq 0$ by (53). If (53) does not hold then it follows that $\bar{Y}_1(X)$ is the horizontal line $Y_1 = \frac{1}{2} \ln \mathcal{A}$. \square

Remark 4.6. *Physically relevant streamlines must lie between (and avoid) the singular points $Q_0^{s,l}$ and $Q_{\pm\pi}^s$, which provides additional physical conditions for the wave-steepness parameters \mathbf{c}, \mathbf{c}_1 . Furthermore $\dot{X} < 0$ along any physically relevant streamline in the (X, Y_1) -plane.*

Remark 4.7. *For $|A| < 1$ and $\mathbf{c} > 0$, the phase portraits share the same essential features as those in the irrotational setting (cf. [20, 21]) whenever $|\mathfrak{R}| > 1$ and (51) holds. A similar observation holds if $|\mathfrak{R}| < 1$ and*

$$\operatorname{arcosh} \frac{1}{|\mathfrak{R}|} - \tanh \operatorname{arcosh} \frac{1}{|\mathfrak{R}|} < \left| \frac{k\mathbf{c}}{\gamma_1} + \frac{1}{2} \ln \mathcal{A} \right|.$$

In particular, for $\gamma_1 > 0$ and $\mathbf{c} > 0$, a transition from 7 to 3 singular points occurs whenever the above relation, and so also (51), become equalities.

4.4.2 $|A| < 1$, and $\mathbf{c} < 0$ (critical layer present)

Proposition 4.6. *For $|A| < 1$, let $\gamma_1 > 0$ be such that $\mathbf{c} < 0$. Suppose $|\mathfrak{R}| < 1$, (51) holds, and also*

$$k\mathbf{c} \neq -\frac{\gamma_1}{2} \ln \mathcal{A}.$$

Then the ∞ -isocline for the dynamical system (36) consists of 3 disjoint parts, and there exist 5 singular points.

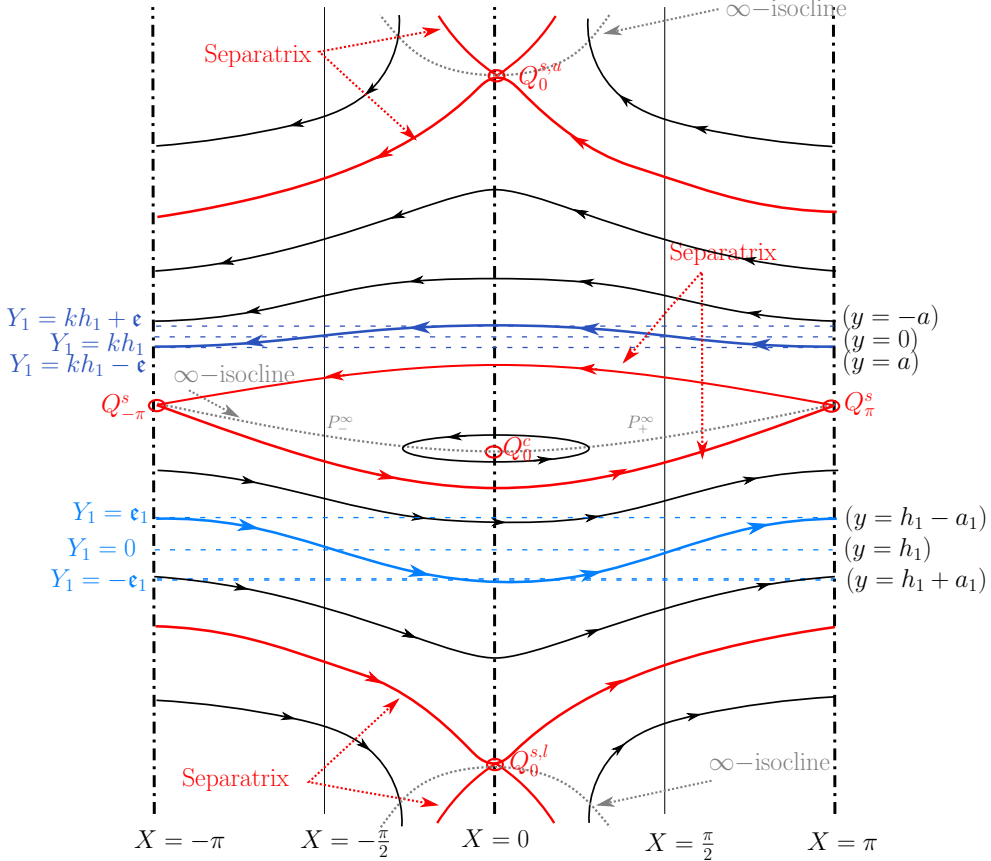


Figure 11: Phase portrait for $A < 1$, $\mathfrak{c} < 0$ and $\gamma_1 > 0$. The schematic corresponds to a regime whereby $\frac{k\mathfrak{c}}{\gamma_1} + \frac{1}{2} \ln \mathcal{A} < 0$. A similar legend applies as in Figure 9.

Proof. First, note that the line $Y_1 = \frac{1}{2} \ln \mathcal{A}$ cannot intersect the ∞ -isocline: for fixed X , we have $F(X, \frac{1}{2} \ln \mathcal{A}) = -k\mathfrak{c} - \frac{\gamma_1}{2} \ln \mathcal{A}$, which is non-zero by assumption. Similarly, the line $Y_1 = 0$ also cannot intersect the ∞ -isocline: $F(X, 0) = M_1 A \cos X - k\mathfrak{c}$ and $M_1 = \mathfrak{e}_1 k\mathfrak{c} \ll k\mathfrak{c}$. In the regime $|A| < 1$, we have $\frac{\partial F}{\partial Y_1} < 0$ for $X \in [-\pi, \pi] \setminus (-\frac{\pi}{2}, \frac{\pi}{2})$ by our assumptions on A and γ_1 . On the other hand, (51) implies that $F(X, Y_1^+(X))F(X, Y_1^-(X)) < 0$ for all X in $(-\frac{\pi}{2}, \frac{\pi}{2})$, and so $F(X, \cdot)$ behaves similarly to $\mathcal{F}(Y_1)$. Consequently, the equation $F(X, Y_1) = 0$ has three solutions for any fixed $X \in (-\frac{\pi}{2}, \frac{\pi}{2})$, and one solution otherwise.

Let $Y_1^*(X) < \bar{Y}_1(X) < \bar{Y}_1^*(X)$ be the three solutions of $F(X, Y_1) = 0$, when $-\frac{\pi}{2} < X < \frac{\pi}{2}$ is fixed. Then, suppressing any X dependence, the relations $Y_1^* < Y_1^- < \bar{Y}_1$ and $\bar{Y}_1 < Y_1^+ < \bar{Y}_1^*$ hold true, as F does not vanish

along Y_1^\pm , by (50) and (51). In particular, we have

$$Y_1^*(X) < Y_1^-(X) < \frac{1}{2} \ln \mathcal{A} < Y_1^+(X) < \bar{Y}_1^*(X) \quad \text{for all } |X| < \frac{\pi}{2},$$

after taking into account (50). If $Y_1(X)$ satisfies $F(X, Y_1(X)) = 0$, then an implicit differentiation yields

$$\frac{d}{dX} F(X, Y_1(X)) = 0 \Leftrightarrow M_1 \sin X f(Y_1(X)) = \frac{\partial Y_1}{\partial X} \frac{\partial F}{\partial Y_1}, \quad (54)$$

for all X_0 , where $\frac{\partial F}{\partial Y_1} = M_1 \cos X g(Y_1(X)) - \gamma_1$. Thus, taking into account $\frac{1}{2} \ln \mathcal{A} < Y_1^+(X) < \bar{Y}_1^*(X)$, Figure 8, and examining (54), we deduce that Y_1^* is a decreasing function for $0 \leq X < \frac{\pi}{2}$, whereas \bar{Y}_1^* is increasing in the same region. The monotonicity of both functions with respect to X is reversed in the region $-\frac{\pi}{2} < X < 0$. Inspecting the limit of $F(X, \bar{Y}_1(X))$, as $X \rightarrow \frac{\pi}{2}^-$, we have $\lim_{X \rightarrow \frac{\pi}{2}^-} \bar{Y}_1(X) = -\frac{k\mathfrak{c}}{\gamma_1}$.

Let \bar{Y}_1 be the unique solution of the equation $F(X, Y_1) = 0$, for fixed X such that $\frac{\pi}{2} \leq |X|$. Revisiting our earlier arguments we deduce that $\lim_{X \rightarrow \frac{\pi}{2}^+} \bar{Y}_1(X) = -\frac{k\mathfrak{c}}{\gamma_1}$. We now examine the relative position of the horizontal line $Y_1 = \frac{1}{2} \ln \mathcal{A}$ and the graph of \bar{Y}_1 . The monotonicity of $F(X, \cdot)$ dictates that, if

$$0 = F(X, \bar{Y}_1(X)) < F\left(X, \frac{1}{2} \ln \mathcal{A}\right) = -k\mathfrak{c} - \frac{\gamma_1}{2} \ln \mathcal{A}$$

holds, then $\bar{Y}_1(X) < \frac{1}{2} \ln \mathcal{A}$, for all $X \in [-\pi, \pi]$. Furthermore, \bar{Y}_1 is increasing for positive X , and decreasing for negative X , due to (54). Analogously, when $\frac{k\mathfrak{c}}{\gamma_1} + \frac{1}{2} \ln \mathcal{A} > 0$, the graph of $\bar{Y}_1(X)$ must lie above the line $Y_1 = \frac{1}{2} \ln \mathcal{A}$ for all $X \in [-\pi, \pi]$, with a reversal in the monotonicity of \bar{Y}_1 .

The singular points for the dynamical system (36) occur at $Q_0^c = (0, \bar{Y}_1(0))$, $Q_0^{s,l} = (0, Y_1^*(0))$, $Q_0^{s,u} = (0, \bar{Y}_1^*(0))$, $Q_{\pm\pi}^s = (\pm\pi, \bar{Y}_1(\pm\pi))$. Since $\frac{\partial F}{\partial Y_1}(0, \bar{Y}_1(0)) = M_1(A \sinh \bar{Y}_1(0) - \cosh \bar{Y}_1(0)) - \gamma_1$, the Hessian (39) at Q_0^c is

$$D^2 H_1(0, \bar{Y}_1(0)) = \begin{pmatrix} -M_1(A \sinh \bar{Y}_1(0) - \cosh \bar{Y}_1(0)) & 0 \\ 0 & \frac{\partial F}{\partial Y_1}(0, \bar{Y}_1(0)) \end{pmatrix}.$$

The first diagonal term is negative, since $M_1 < 0$ and $A < 1$, and the second diagonal term is also negative due to monotonicity considerations: hence Morse theory implies that $Q_0^c = (0, \bar{Y}_1(0))$ is a centre. Monotonicity considerations (cf. Figure 8) imply $\frac{\partial F}{\partial Y_1}(0, Y_1^*(0)), \frac{\partial F}{\partial Y_1}(0, \bar{Y}_1^*(0)) > 0$, hence

similar arguments imply that $Q_0^{s,l} = (0, Y_1^*(0))$ and $Q_0^{s,u} = (0, \bar{Y}_1^*(0))$ are saddle points. Finally,

$$D^2 H_1(\pi, \bar{Y}_1(\pi)) = \begin{pmatrix} M_1 g(\bar{Y}_1(\pi)) & 0 \\ 0 & -g(\bar{Y}_1(\pi)) - \gamma_1 \end{pmatrix},$$

with the Hessian matrix having the same form when $X = -\pi$. Noting that $M_1 < 0$, $A < 1$, and $\frac{\partial F}{\partial Y_1}(\pi, \bar{Y}_1(\pi)) = -g(\bar{Y}_1(\pi)) - \gamma_1$, it follows that $Q_{\pm\pi}^s = (\pm\pi, \bar{Y}_1(\pm\pi))$ correspond to saddle points. \square

Remark 4.8. *In the presence of the critical layer, and bearing in mind the monotonicity of $F(X, \cdot)$, the existence of physically admissible solutions of (36) corresponding to streamlines of the upper-fluid layer is equivalent to the conditions $F(0, Y_1^*(0)) < F(0, -\epsilon_1)$ and $F(0, kh_1 - \epsilon) < F(0, \bar{Y}_1^*(0))$ holding.*

4.5 The case $A > 1$

For $A > 1$ we have

$$\frac{a}{a_1} \frac{c}{\epsilon} < e^{-kh_1}, \quad (55)$$

since the right-hand side of (27) is a decreasing function of A . For $\epsilon > 0$, we may equivalently express (55) as

$$\gamma_1 < \frac{c}{h_1} \left(1 - \frac{a}{a_1} e^{kh_1} \right),$$

with the reverse inequality holding for $\epsilon < 0$. These relations are useful for immediately inferring various basic properties of the wave solutions. For instance, if $\gamma_1 > 0$ is such that $\epsilon > 0$, then we can have either in-phase waves with the restriction $a < a_1 \epsilon e^{-kh_1} / c$ (noting that $\epsilon/c < 1$ in this regime), or else out-of-phase waves. Regarding the existence of out-of-phase waves in this regime (that is, in the absence of critical layers) for $A > 1$ it follows from direct calculation that

$$g(Y_1) = A \sinh Y_1 - \cosh Y_1 = 0 \iff Y_1 = \frac{1}{2} \ln \tilde{\mathcal{A}},$$

where we denote $\tilde{\mathcal{A}} := \frac{A+1}{A-1}$. Hence, when $A > 1$, the horizontal line $Y_1 = \frac{1}{2} \ln \tilde{\mathcal{A}}$ demarcates a change in direction in the vertical velocity for the dynamical system (36). Consequently, even in the absence of critical layers (and associated flow reversal) out-of-phase waves (whereby $a < 0$) will occur if $\frac{1}{2} \ln \tilde{\mathcal{A}} < kh_1$: this is in contrast to the previously considered situations when $A \leq 1$. The phase-plane analysis we perform below furnishes us with

an elegant and explicit visualisation of the transition process from in-phase, to out-of-phase, internal-surface wave coupling.

The 0-isocline of the dynamical system (36), which consists of the points for which $\dot{Y}_1 = G(X, Y_1) = M_1 \sin X g(Y_1) = 0$, comprises the vertical lines $X = 0, \pm\pi$, and the horizontal line $Y_1 = \frac{1}{2} \ln \tilde{\mathcal{A}}$. The ∞ -isocline of the dynamical system (36) consists of points for which $\dot{X} = F(X, Y_1) = M_1 \cos X f(Y_1) - k\mathbf{c} - \gamma_1 Y_1 = 0$, where $f(Y_1) = A \cosh Y_1 - \sinh Y_1$. As before, the points $P_{\pm}^{\infty} = \left(\pm\frac{\pi}{2}, -\frac{k\mathbf{c}}{\gamma_1}\right)$ in (38) will be in the ∞ -isocline. Qualitative features of the ∞ -isocline can be determined by considering, for fixed X , the monotonicity properties of $F(X, \cdot)$ via $\frac{\partial F}{\partial Y_1} = M_1 \cos X g(Y_1) - \gamma_1$. Since $g(Y_1)$ is a strictly increasing function of Y_1 for $A > 1$, it follows that if $M_1 \cos X > 0$, then $F(X, \cdot)$ is strictly decreasing until it reaches its minimum value Y_1^+ , from which point it is strictly increasing: $F(X, \cdot)$ has monotonicity properties similar to $\tilde{\mathcal{F}}(Y_1)$ in Figure 12; if $M_1 \cos X < 0$, the reverse scenario occurs, with $F(X, \cdot)$ having similar monotonicity properties as $-\tilde{\mathcal{F}}(Y_1)$ in Figure 12. Hence, for a given X , the ∞ -isocline contains points with abscissa X if $F(X, \cdot)$ intersects the Y_1 -axis, which is equivalent to $F(X, Y_1^+)$ either touching the Y_1 -axis, or else lying on the opposite side to the Y_1 -axis as the asymptotic values of $F(X, \cdot)$: the latter scenario is depicted in Figure 12.

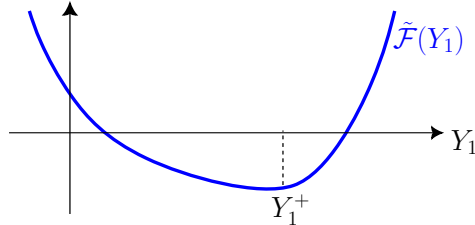


Figure 12: The function $\tilde{\mathcal{F}}(Y_1)$, when $A > 1$.

The extremum value Y_1^+ for $F(X, \cdot)$ can be computed (for $X \neq \frac{\pi}{2}$) from

$$\begin{aligned} \frac{\partial F}{\partial Y_1}(X, Y_1^+(X)) = 0 &\iff g(Y_1^+) = A \sinh Y_1^+ - \cosh Y_1^+ = \frac{\gamma_1}{M_1 \cos X} \\ &\iff (A - 1) \left(e^{Y_1^+} \right)^2 - \frac{2\gamma_1}{M_1 \cos X} e^{Y_1^+} - (A + 1) = 0 \\ &\iff e^{Y_1^+} = \sqrt{\tilde{\mathcal{A}}} \left(s + \sqrt{s^2 + 1} \right), \quad s = \frac{\gamma_1}{M_1 \cos X \sqrt{A^2 - 1}}. \end{aligned}$$

Using the relation $\text{arsinh}(s) = \ln(s + \sqrt{s^2 + 1})$ we get, for $X \neq \pm\frac{\pi}{2}$,

$$Y_1^+(X) = \frac{1}{2} \ln \tilde{\mathcal{A}} + \text{arsinh } z_2(X), \text{ for } z_2(X) := \frac{\gamma_1}{M_1 \cos X \sqrt{A^2 - 1}}. \quad (56)$$

Note that since $g(Y_1)$ is an increasing function it follows that (for $X \neq \pm\frac{\pi}{2}$)

$$\begin{aligned} Y_1^+(X) < 0 &\iff \sqrt{\tilde{\mathcal{A}}} \left(z_2(X) + \sqrt{z_2^2(X) + 1} \right) < 1 \\ &\iff \frac{\gamma_1}{M_1 \cos X} = g(Y_1^+) < g(0) = -1, \end{aligned}$$

where we note that the second relation implies that $z_2(X) < 0$. Since (27) implies that $\frac{a}{a_1} \frac{c}{\mathfrak{c}} = -g(kh_1)$, it follows that

$$Y_1^+(X) > kh_1 \iff \frac{\gamma_1}{M_1 \cos X} = g(Y_1^+) > g(kh_1) = -\frac{a}{a_1} \frac{c}{\mathfrak{c}}.$$

Furthermore, Y_1^+ never intersects the 0-isocline given by the line $Y_1 = \frac{1}{2} \ln \tilde{\mathcal{A}}$ (as $z_2(X) \neq 0$), and $\lim_{X \rightarrow \pm\frac{\pi}{2}} |Y_1^+(X)| = \infty$. Using hyperbolic function identities, and the fact that $f(\frac{1}{2} \ln \tilde{\mathcal{A}}) = \sqrt{A^2 - 1}$ and $g(\frac{1}{2} \ln \tilde{\mathcal{A}}) = 0$, we get

$$\begin{aligned} F(X, Y_1^+(X)) &= M_1 \cos X f(\tilde{\mathcal{A}}) \cosh \text{arsinh } z_2(X) - k\mathfrak{c} - \gamma_1 Y_1^+ \\ &= M_1 \cos X \sqrt{A^2 - 1} \sqrt{z_2(X)^2 + 1} - k\mathfrak{c} - \gamma_1 Y_1^+ \\ &= \gamma_1 \left(\frac{\sqrt{z_2(X)^2 + 1}}{z_2(X)} - \text{arsinh } z_2(X) - \frac{k\mathfrak{c}}{\gamma_1} - \frac{1}{2} \ln \tilde{\mathcal{A}} \right) \\ &= \gamma_1 \left(\coth \text{arsinh } z_2(X) - \text{arsinh } z_2(X) - \frac{k\mathfrak{c}}{\gamma_1} - \frac{1}{2} \ln \tilde{\mathcal{A}} \right), \end{aligned} \quad (57)$$

using the identities $\cosh \text{arsinh } s = \sqrt{s^2 + 1}$ and $\coth \text{arsinh } s = \frac{\sqrt{s^2 + 1}}{s}$ ($s \neq 0$). The function $s \mapsto \coth s - s$ is such that $\lim_{s \rightarrow \pm\infty} \coth s - s = \mp\infty$, therefore, for values of X close to $\frac{\pi}{2}$, $F(X, Y_1^+)$ must take the opposite sign to the asymptotic values of $F(X, Y_1)$, implying that the equation $F(X, Y_1) = 0$ has two solutions in Y_1 (and so the ∞ -isocline has two branches in this region). Finally, the definition of z_2 in (56), together with (57), imply that

$$F(X + \pi, Y_1^+(X + \pi)) = -F(X, Y_1^+(X)) - 2 \left(k\mathfrak{c} + \frac{\gamma_1}{2} \ln \tilde{\mathcal{A}} \right), \quad X \neq \pm\frac{\pi}{2}. \quad (58)$$

4.5.1 $A > 1$ and $\mathfrak{c} > 0$ (no critical layers)

Proposition 4.7. For $A > 1$, let $\gamma_1 > 0$ be such that $\mathfrak{c} > 0$. If

$$F(\pi, Y_1^+(\pi)) > 0, \quad (59)$$

and

$$F(0, -\mathfrak{c}_1) < 0 \quad (60)$$

are satisfied, then the dynamical system (36) has 6 singular points.

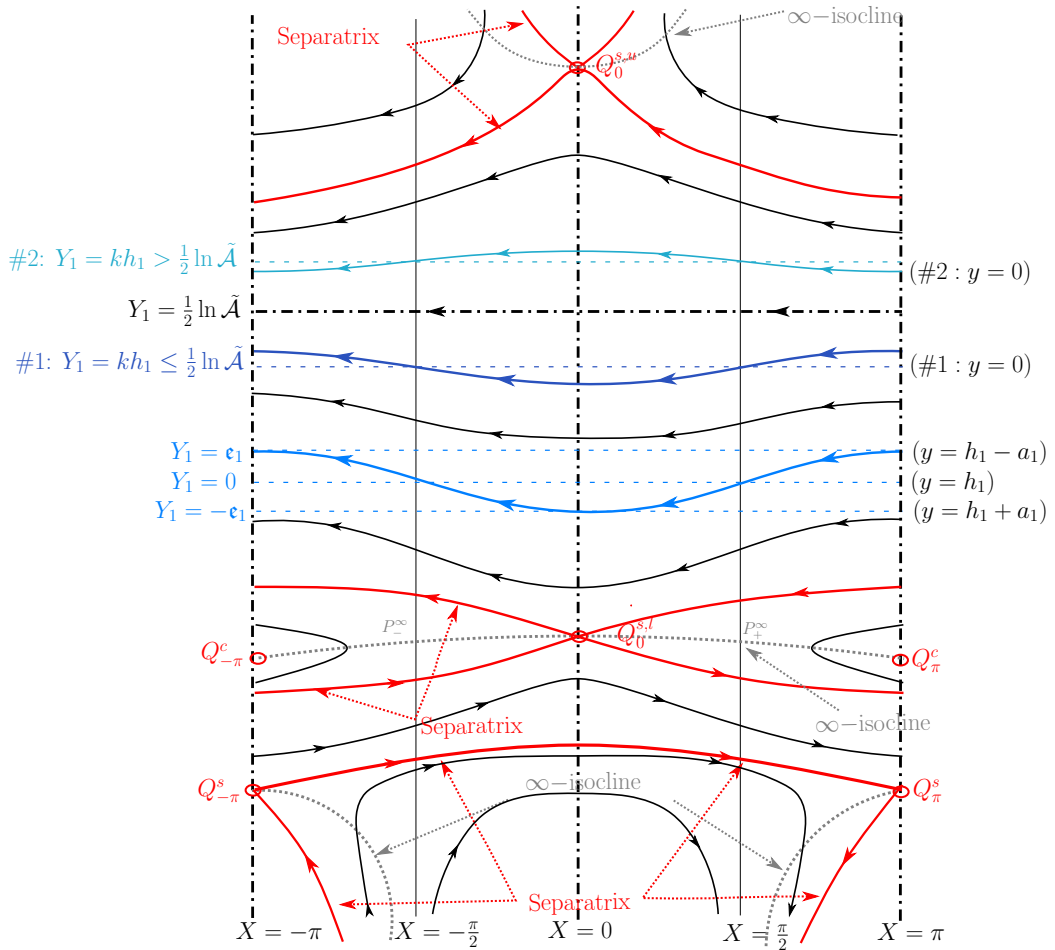


Figure 13: Phase portrait for $A > 1$, $\mathfrak{c} > 0$, $\gamma_1 > 0$, where (59) and (60) hold. The dotted grey lines represent ∞ -isoclines, with the dotted-dashed lines - - - representing 0-isoclines. The surface wave profile (—) has mean-water level $Y_1 = 0$, corresponding to $y = h_1$. The internal wave profile is illustrated for two differing values of the mean water level $Y = kh_1$, corresponding to $y = 0$: $kh_1 \leq \bar{Y}_1$ in Case 1 (—), whereas $kh_1 > \bar{Y}_1$ for Case 2 (—).

Proof. As discussed in the previous Section, since $M_1 = \epsilon_1 k \mathfrak{c} > 0$ the behaviour of $F(X, \cdot)$ is similar to that of $\tilde{\mathcal{F}}$ depicted in Figure 12 when $|X| < \frac{\pi}{2}$, and similar to that of $-\tilde{\mathcal{F}}$ when $|X| \in (\frac{\pi}{2}, \pi]$. For X in the latter region (with $\cos X < 0$), we claim that $F(X, Y_1^+(X)) > 0$ holds, where $\frac{\partial F}{\partial Y_1}(X, Y_1^+(X)) = 0$. This follows from noting that (59) can be reexpressed

$$\operatorname{arsinh} \frac{1}{\tilde{\mathfrak{R}}} - \coth \operatorname{arsinh} \frac{1}{\tilde{\mathfrak{R}}} > \frac{k \mathfrak{c}}{\gamma_1} + \frac{1}{2} \ln \tilde{\mathcal{A}}, \quad \text{for } \tilde{\mathfrak{R}} := \frac{M_1 \sqrt{A^2 - 1}}{\gamma_1},$$

coupled with the observation that the function $X \mapsto \coth \operatorname{arsinh} \frac{1}{\tilde{\mathfrak{R}} \cos X} - \operatorname{arsinh} \frac{1}{\tilde{\mathfrak{R}} \cos X}$ restricted to the interval $[-\pi, -\frac{\pi}{2})$ attains its minimum at $x_0 = -\pi$. Consequently, for fixed X such that $|X| \in (\frac{\pi}{2}, \pi]$, the equation $F(X, Y_1) = 0$ has two solutions with respect to Y_1 . We can then apply (58) directly to infer that the reverse scenario, $F(X, Y_1^+(X)) < 0$, holds for X in the region $|X| < \frac{\pi}{2}$. This proves that, for any fixed $X \neq \pm \frac{\pi}{2}$, the equation $F(X, Y_1) = 0$ has two solutions with respect to the Y_1 variable. Since $\frac{\partial F}{\partial Y_1}$ vanishes only along Y_1^+ and $F(X, Y_1^+(X)) \neq 0$, the implicit function theorem implies that we can write the solutions as functions of X . For $|X| \in (\frac{\pi}{2}, \pi]$ we denote these solutions by $Y_1^*(X) < Y_1^+(X) < \bar{Y}_1(X)$, whereas for $|X| < \frac{\pi}{2}$ we denote the solutions as $\bar{Y}_1(X) < Y_1^+(X) < Y_1^*(X)$.

If we define $\bar{Y}_1(\pm \frac{\pi}{2}) = -\frac{k \mathfrak{c}}{\gamma_1}$, then $\bar{Y}_1(X)$ defines a curve which extends across the entire domain $[-\pi, \pi]$. The monotonicity of \bar{Y}_1 can be established from its slope which is prescribed by

$$\frac{d}{dX} F(X, \bar{Y}_1(X)) = 0 \Leftrightarrow M_1 \sin X f(\bar{Y}_1(X)) = \frac{\partial \bar{Y}_1}{\partial X} (M_1 \cos X g(\bar{Y}_1(X)) - \gamma_1),$$

which allows us to deduce that \bar{Y}_1 is decreasing when $X_0 \in (0, \pi)$, and increasing when $X_0 \in (-\pi, 0)$. Since $-\frac{k \mathfrak{c}}{\gamma_1} < 0$, this implies that $\bar{Y}_1(X)$ must lie beneath the upper fluid domain, in terms of (X, Y_1) coordinates, for $|X| \leq \frac{\pi}{2}$. Furthermore, (60) implies that $\bar{Y}_1(0) < -\epsilon_1$, and the monotonicity properties of the free-surface streamline, allied to those of $\bar{Y}_1(X)$, imply that $\bar{Y}_1(X)$ also lies beneath the upper fluid domain, in terms of (X, Y_1) coordinates, for $|X| \in (\frac{\pi}{2}, \pi]$.

Bearing in mind the form of the 0-isocline, there exist singular points at $Q_{\pm\pi}^s = (\pm\pi, Y_1^*(\pm\pi))$ and $Q_{\pm\pi}^c = (\pm\pi, \bar{Y}_1(\pm\pi))$ (recalling that $Y_1^*(\pi) < Y_1^+(\pi) < \bar{Y}_1(\pi)$) as well as at $Q_0^{s,l} = (0, \bar{Y}_1(0))$ and $Q_0^{s,u} = (0, \bar{Y}_1^*(0))$ (where $\bar{Y}_1(0) < Y_1^+(0) < \bar{Y}_1^*(0)$). There are no other singular points since the ∞ -isocline does not intersect the horizontal line $Y_1 = \frac{1}{2} \ln \tilde{\mathcal{A}}$: we have already established that $\bar{Y}_1(X) < 0 < \frac{1}{2} \ln \tilde{\mathcal{A}}$ in the entire domain, and $Y_1^*(X) < Y_1^+(X) < \bar{Y}_1(X)$ in $|X| \in (\frac{\pi}{2}, \pi]$; while in the region $|X| \leq \frac{\pi}{2}$ we have $\bar{Y}_1^*(X) > Y_1^+(X) > \frac{1}{2} \ln \tilde{\mathcal{A}}$, where the latter inequality follows from (56).

We examine the Hessian of the Hamiltonian H_1 at the singular points. For $Q_0^{s,l} = (0, \bar{Y}_1(0))$ we have

$$D^2 H_1(0, \bar{Y}_1(0)) = \begin{pmatrix} -M_1 g(\bar{Y}_1(0)) & 0 \\ 0 & M_1 g(\bar{Y}_1(0)) - \gamma_1 \end{pmatrix}.$$

The first diagonal term is positive, as $M_1 > 0$ and $\bar{Y}_1(0) < \frac{1}{2} \ln \tilde{\mathcal{A}}$, while previously outlined monotonicity considerations imply that the second term in the diagonal is negative, therefore Morse theory implies that $Q_0^{s,l} = (0, \bar{Y}_1(0))$ is a saddle point. For $Q_0^{s,u} = (0, \bar{Y}_1^*(0))$ we have

$$D^2 H_1(0, \bar{Y}_1^*(0)) = \begin{pmatrix} -M_1 g(\bar{Y}_1^*(0)) & 0 \\ 0 & M_1 g(\bar{Y}_1^*(0)) - \gamma_1 \end{pmatrix},$$

and since $\frac{1}{2} \ln \tilde{\mathcal{A}} < Y_1^+(0) < \bar{Y}_1^*(0)$ we have $-M_1 g(\bar{Y}_1^*(0)) < 0$, with the monotonicity properties yielding the claim. For $Q_\pi^s = (\pi, Y_1^*(\pi))$ we have

$$D^2 H_1(\pi, Y_1^*(\pi)) = \begin{pmatrix} M_1 g(Y_1^*(\pi)) & 0 \\ 0 & -M_1 g(Y_1^*(\pi)) - \gamma_1 \end{pmatrix},$$

the first diagonal term is negative since $Y_1^*(\pi) < 0 < \frac{1}{2} \ln \tilde{\mathcal{A}}$, while monotonicity properties imply that the second term in the main diagonal is positive: $Q_\pi^{s,u} = (\pi, Y_1^*(\pi))$ corresponds to a saddle point. For $Q_\pi^c = (\pi, \bar{Y}_1(\pi))$,

$$D^2 H_1(\pi, \bar{Y}_1(\pi)) = \begin{pmatrix} M_1 g(\bar{Y}_1(\pi)) & 0 \\ 0 & -M_1 g(\bar{Y}_1(\pi)) - \gamma_1 \end{pmatrix}.$$

Taking into account the fact that $Y_1^+(\pi) < \bar{Y}_1(\pi) < \frac{1}{2} \ln \tilde{\mathcal{A}}$, and using monotonicity properties once more, we can deduce from Morse theory that $Q_\pi^c = (\pi, \bar{Y}_1(\pi))$ corresponds to a centre. We note that since the upper fluid domain lies between the separatrices which emanate from $Q_0^{s,l}$, and $Q_0^{s,u}$, respectively, we have $\dot{X} < 0$ along physically relevant streamlines. \square

Remark 4.9. *The arguments of Proposition 4.7 imply that 2 saddle-centre bifurcations occur when*

$$F(\pi, Y_1^+(\pi)) = 0 \iff \operatorname{arsinh} \frac{1}{\tilde{\mathfrak{R}}} - \coth \operatorname{arsinh} \frac{1}{\tilde{\mathfrak{R}}} = \frac{k\mathfrak{c}}{\gamma_1} + \frac{1}{2} \ln \tilde{\mathcal{A}},$$

with a resulting transition from 6 to 2 critical points.

Proposition 4.8. *For $A > 1$, let $\gamma_1 < 0$ (and so $\mathfrak{c} > 0$). Let $\mathcal{M} = \max\{kh_1 - \mathfrak{c}, \frac{1}{2} \ln \tilde{\mathcal{A}}\}$. If*

$$F(\pi, Y_1^+(\pi)) > 0, \tag{61}$$

and

$$F(0, \mathcal{M}) < 0, \quad F(0, -\mathfrak{e}) < 0, \quad (62)$$

are satisfied, then the dynamical system (36) has 6 singular points.

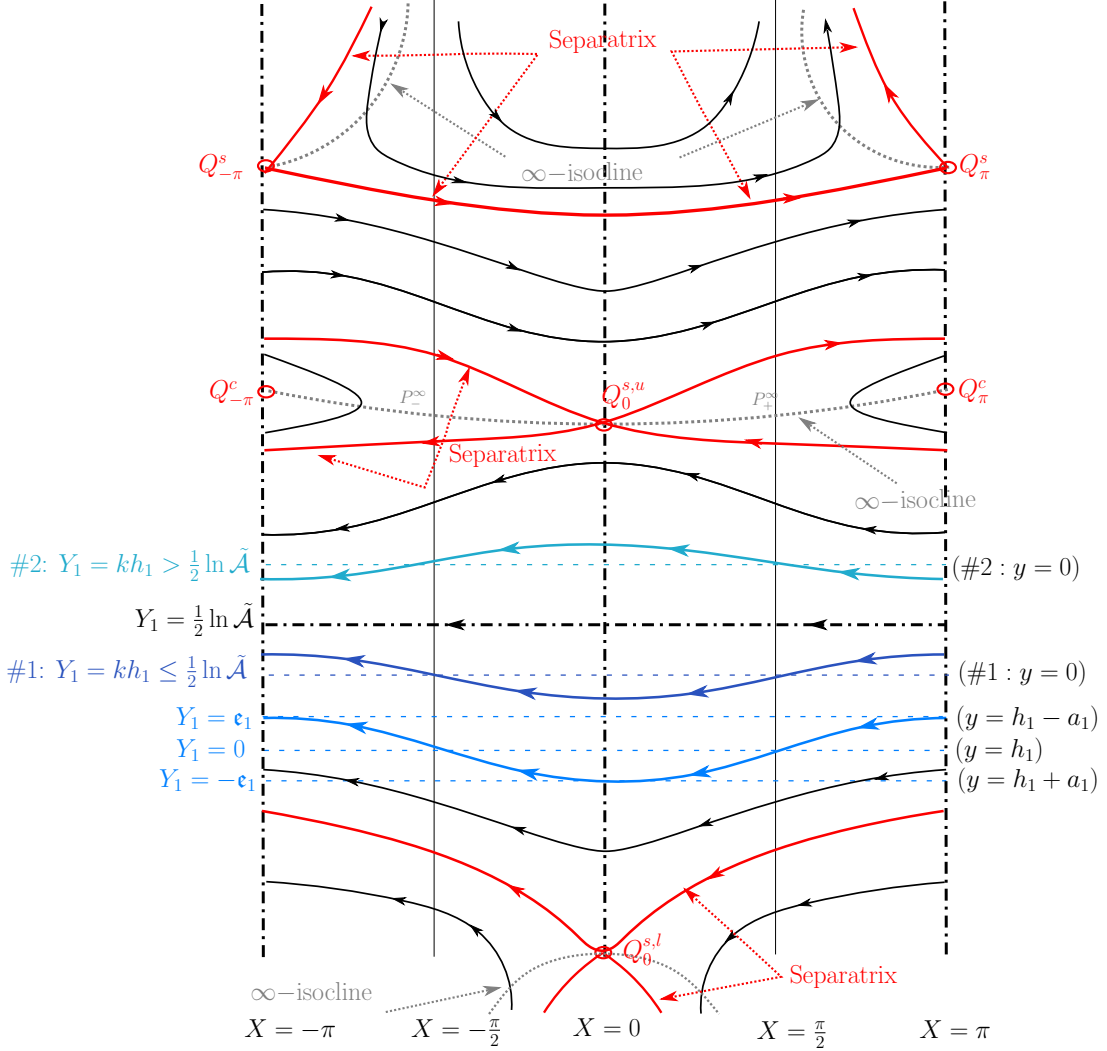


Figure 14: Phase portrait for $A > 1$, $\gamma_1 < 0$ ($\mathfrak{c} > 0$), where (61) and (62) hold. A similar legend applies as in Figure 13.

Proof. Condition (61) can be expressed as

$$F(\pi, Y_1^+(\pi)) > 0 \iff \operatorname{arsinh} \frac{1}{\tilde{\mathfrak{R}}} - \coth \operatorname{arsinh} \frac{1}{\tilde{\mathfrak{R}}} < \frac{k\mathfrak{c}}{\gamma_1} + \frac{1}{2} \ln \tilde{\mathcal{A}},$$

and it is clear from the functional form of (57) that a similar inequality, $F(X, Y_1^+(X)) > 0$, will hold for all $|X| \in (\frac{\pi}{2}, \pi]$ since $\tilde{\Re} < 0$. Condition (62) implies that $F(0, Y_1^+(0)) < 0$, which can be reexpressed as

$$F(0, Y_1^+(0)) < 0 \iff \coth \operatorname{arsinh} \frac{1}{\tilde{\Re}} - \operatorname{arsinh} \frac{1}{\tilde{\Re}} > \frac{k\mathfrak{c}}{\gamma_1} + \frac{1}{2} \ln \tilde{\mathcal{A}}.$$

From $\tilde{\Re} < 0$, and the functional form of (57), it is clear that $F(X, Y_1^+(X)) < 0$ will hold for all $|X| < \frac{\pi}{2}$. Therefore the equation $F(X, Y_1) = 0$ has two solutions with respect to Y_1 for all $X \neq \frac{\pi}{2}$, and since $\frac{\partial F}{\partial Y_1}$ vanishes only along Y_1^+ and $F(X, Y_1^+(X)) \neq 0$, the implicit function theorem implies that we can write the solutions as functions of X . For $|X| \in (\frac{\pi}{2}, \pi]$ we denote these solutions by $\bar{Y}_1(X) < Y_1^+(X) < Y_1^*(X)$, whereas for $|X| < \frac{\pi}{2}$ we denote the solutions as $\bar{Y}_1^*(X) < Y_1^+(X) < \bar{Y}_1(X)$ (note the reversal in ordering compared to Proposition 4.7).

We again set $\bar{Y}_1(\pm\frac{\pi}{2}) = -\frac{k\mathfrak{c}}{\gamma_1}$, in which case $\bar{Y}_1(X)$ defines a curve which extends across the entire domain $[-\pi, \pi]$. Similar to Proposition 4.7, we can establish monotonicity properties for \bar{Y}_1 , except now \bar{Y}_1 is increasing when $X_0 \in (0, \pi)$, and decreasing for $X_0 \in (-\pi, 0)$. Since $-\frac{k\mathfrak{c}}{\gamma_1} = -\frac{k\mathfrak{c}}{\gamma_1} + kh_1 > kh_1 > 0$, as $\gamma_1 < 0$, it follows that $\bar{Y}_1(X)$ lies above the upper-fluid layer for $|X| \in [\frac{\pi}{2}, \pi]$. Indeed, the first inequality in (62) implies that $\bar{Y}_1(0) > kh_1 - \mathfrak{c}$, $\bar{Y}_1(0) > \frac{1}{2} \ln \tilde{\mathcal{A}}$ (where we note that $kh_1 - \mathfrak{c} > \frac{1}{2} \ln \tilde{\mathcal{A}}$ only when waves are out-of-phase, in which case $\mathfrak{c} < 0$) and the monotonicity properties of the internal-wave streamline, allied to those of $\bar{Y}_1(X)$, imply that $\bar{Y}_1(X)$ must lie above the upper fluid domain, in terms of (X, Y_1) coordinates, for $|X| \leq \frac{\pi}{2}$.

Due to the form of the 0-isocline there exist singular points at $Q_0^{s,l} = (0, \bar{Y}_1^*(0))$, $Q_0^{s,u} = (0, \bar{Y}_1(0))$ (where $\bar{Y}_1^*(0) < Y_1^+(0) < \bar{Y}_1(0)$), and $Q_{\pm\pi}^s = (\pm\pi, Y_1^*(\pm\pi))$, $Q_{\pm\pi}^c = (\pm\pi, \bar{Y}_1(\pm\pi))$ (with $\bar{Y}_1(\pi) < Y_1^+(\pi) < Y_1^*(\pi)$). There are no other singular points since we have shown that $\bar{Y}_1(X)$ lies above the horizontal line $Y_1 = \frac{1}{2} \ln \tilde{\mathcal{A}}$, with $Y_1^*(X) > \bar{Y}_1(X)$ for $|X| \in [\frac{\pi}{2}, \pi]$, while the second inequality in condition (62) implies that $\bar{Y}_1^*(X) < 0$: therefore the ∞ -isocline cannot intersect the 0-isocline along the line $Y_1 = \frac{1}{2} \ln \tilde{\mathcal{A}}$.

We examine the Hessian of the Hamiltonian H_1 at the singular points. At $Q_0^{s,u} = (0, \bar{Y}_1(0))$ we have

$$D^2 H_1(0, \bar{Y}_1(0)) = \begin{pmatrix} -M_1 g(\bar{Y}_1(0)) & 0 \\ 0 & M_1 g(\bar{Y}_1(0)) - \gamma_1 \end{pmatrix},$$

where the first diagonal term is negative, as $M_1 > 0$ and $\bar{Y}_1(X) > \frac{1}{2} \ln \tilde{\mathcal{A}}$, while monotonicity considerations imply that the second diagonal term is

positive: Morse theory gives that $Q_0^{s,u} = (0, \bar{Y}_1(0))$ is a saddle point. Similarly, at $Q_0^{s,l} = (0, \bar{Y}_1^*(0))$ we have

$$D^2 H_1(0, \bar{Y}_1^*(0)) = \begin{pmatrix} -M_1 g(\bar{Y}_1^*(0)) & 0 \\ 0 & M_1 g(\bar{Y}_1^*(0)) - \gamma_1 \end{pmatrix},$$

and since $Y_1^*(X) < 0 < \ln \mathcal{A}$ the first diagonal term is positive, and monotonicity properties imply that the second term in the main diagonal is negative: $Q_0^{s,l} = (0, \bar{Y}_1^*(0))$ corresponds to a saddle point. For $Q_\pi^c = (\pi, \bar{Y}_1(\pi))$,

$$D^2 H_1(\pi, \bar{Y}_1(\pi)) = \begin{pmatrix} M_1 g(\bar{Y}_1(\pi)) & 0 \\ 0 & -M_1 g(\bar{Y}_1(\pi)) - \gamma_1 \end{pmatrix},$$

and the fact that $\bar{Y}_1(\pi) > \ln \mathcal{A}$, coupled with monotonicity properties, implies that $(\pi, \bar{Y}_1(\pi))$ corresponds to a centre, due to Morse theory. Finally, at $Q_\pi^s = (\pi, Y_1^*(\pi))$ we have

$$D^2 H_1(\pi, Y_1^*(\pi)) = \begin{pmatrix} M_1 g(Y_1^*(\pi)) & 0 \\ 0 & -M_1 g(Y_1^*(\pi)) - \gamma_1 \end{pmatrix},$$

and since $\frac{1}{2} \ln \tilde{\mathcal{A}} < Y_1^*(\pi)$ the first main diagonal term is positive, with the second diagonal term negative due to monotonicity properties: hence $Q_\pi^s = (\pi, Y_1^*(\pi))$ is a saddle. \square

Remark 4.10. *It follows from the arguments of Proposition 4.8 that 2 saddle-centre bifurcations occur when*

$$F(\pi, Y_1^+(\pi)) = 0 \iff \operatorname{arsinh} \frac{1}{\tilde{\mathcal{R}}} - \coth \operatorname{arsinh} \frac{1}{\tilde{\mathcal{R}}} = \frac{k\mathfrak{c}}{\gamma_1} + \frac{1}{2} \ln \tilde{\mathcal{A}},$$

in which case there is a transition from 6 to 2 critical points.

4.5.2 $A > 1$, and $\mathfrak{c} < 0$ (critical layer present)

Proposition 4.9. *For $A > 1$, let $\gamma_1 > 0$ be such that $\mathfrak{c} < 0$. Suppose that the conditions*

$$F\left(\pi, \frac{1}{2} \ln \tilde{\mathcal{A}}\right) < 0 \tag{63}$$

and

$$F(0, Y_1^+(0)) > 0 \tag{64}$$

are satisfied. Then the ∞ -isocline for the dynamical system (36) consists of 4 disjoint parts, and there exist 6 singular points for (36), with 3 of them forming a critical layer.

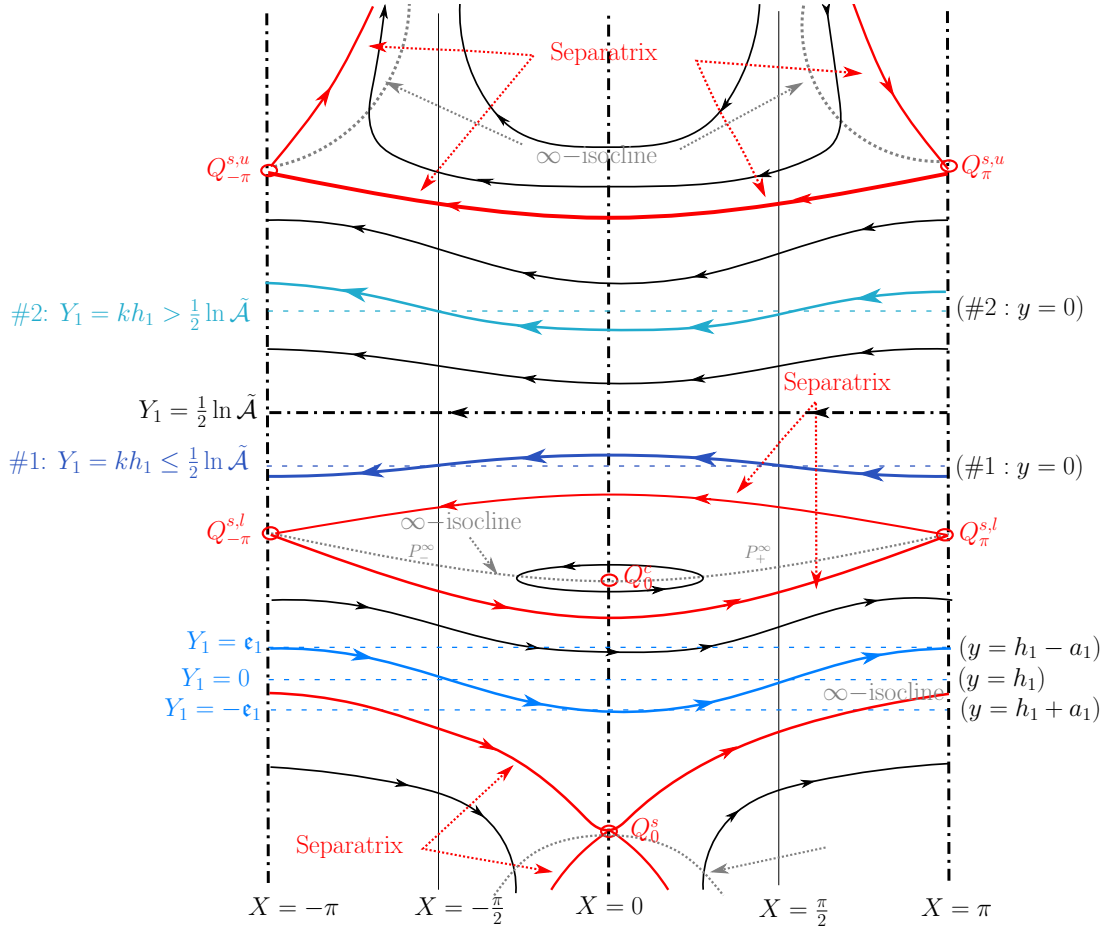


Figure 15: Phase portrait for $A > 1$, $\mathfrak{c} < 0$ and $\gamma_1 > 0$, where conditions (63) and (64) hold. A similar legend applies as in Figure 13.

Proof. Since $c < 0$ we now have $M_1 < 0$ and, as the sign of $M_1 \cos X$ determines the monotonicity properties of $F(X, \cdot)$, it follows that $F(X, \cdot)$ is qualitatively similar to the function $\tilde{\mathcal{F}}(Y_1)$ depicted in Figure 12 for $|X| \in (\frac{\pi}{2}, \pi]$, and qualitatively similar to $-\tilde{\mathcal{F}}(Y_1)$ for $|X| < \frac{\pi}{2}$. We claim that condition (64) implies that $F(X, Y_1^+(X)) > 0$ for $|X| < \frac{\pi}{2}$. Rewriting (64) as

$$\coth \operatorname{arsinh} z_2(0) - \operatorname{arsinh} z_2(0) > \frac{k\mathfrak{c}}{\gamma_1} + \frac{1}{2} \ln \tilde{\mathcal{A}},$$

we note that z_2 is decreasing when $X \in [0, \frac{\pi}{2})$ (since $\gamma_1 > 0$, $M_1 < 0$) and so $\coth \operatorname{arsinh} z_2(\cdot) - \operatorname{arsinh} z_2(\cdot)$ is an increasing function in this range, thereby proving our claim. Bearing in mind the monotonicity properties of $F(X, \cdot)$ for fixed $|X| < \frac{\pi}{2}$, it follows that there are two solutions of $F(X, Y_1) = 0$ with

respect to the Y_1 variable for X in this range. Condition (63) implies that

$$k\mathfrak{c} + \frac{\gamma_1}{2} \ln \tilde{\mathcal{A}} > -M_1 \sqrt{A^2 - 1} > 0, \quad (65)$$

and applying (58) now gives us that $F(X, Y_1^+(X)) < 0$ for all $|X| \in (\frac{\pi}{2}, \pi]$. This fact, coupled with the monotonicity properties of $F(X, \cdot)$, imply that there are two solutions of $F(X, Y_1) = 0$ with respect to the Y_1 variable for fixed X in this range. Since $\frac{\partial F}{\partial Y_1}$ vanishes only along Y_1^+ and $F(X, Y_1^+(X)) \neq 0$, the implicit function theorem implies that we can write these solutions as functions of X .

Let us denote the branches of the ∞ -isocline by $Y_1^*(X) < Y_1^+(X) < \bar{Y}_1(X)$, when $|X| < \frac{\pi}{2}$, and $\bar{Y}_1(X) < Y_1^+(X) < Y_1^*(X)$ for $|X| \in (\frac{\pi}{2}, \pi]$. Recalling (56), and taking the signs of γ_1 and \mathfrak{c} into account, we observe that Y_1^+ takes its maximum value in the interval $(-\frac{\pi}{2}, \frac{\pi}{2})$ at $X_0 = 0$. Thus, for $|X| < \frac{\pi}{2}$, we know that $Y_1^*(X) < Y_1^+(0)$. Combining the last inequality with (56) and (64), we have

$$\begin{aligned} Y_1^*(X) < Y_1^+(0) &= \frac{1}{2} \ln \tilde{\mathcal{A}} + \operatorname{arsinh} z_2(0) \\ &< \coth \operatorname{arsinh} z_2(0) - \frac{k\mathfrak{c}}{\gamma_1} < -\frac{k\mathfrak{c}}{\gamma_1}, \quad \text{for } |X| < \frac{\pi}{2}. \end{aligned}$$

Hence $Y_1^*(X)$ remains below $Y_1 = -\frac{k\mathfrak{c}}{\gamma_1}$. We set $\bar{Y}_1(\frac{\pi}{2}) = -\frac{k\mathfrak{c}}{\gamma_1}$, ensuring that \bar{Y}_1 is well-defined for all $X \in [-\pi, \pi]$. From (54), we have

$$M_1 \sin X f(\bar{Y}_1(X)) = \frac{\partial \bar{Y}_1}{\partial X} (M_1 \cos X g(\bar{Y}_1(X)) - \gamma_1),$$

for $X \in [-\pi, \pi]$. It follows that $\bar{Y}_1(X)$ is increasing for $X \in (0, \pi)$, and $\bar{Y}_1(X)$ is decreasing for $X \in (-\pi, 0)$: hence $\bar{Y}_1(X)$ attains its minimum at $X = 0$, and its maximum at $X = \pm\pi$.

Bearing in mind the nature of the 0-isocline for (36), there are singular points at $Q_0^s = (0, Y_1^*(0))$, $Q_0^c = (0, \bar{Y}_1(0))$, $Q_{\pm\pi}^{s,l} = (\pm\pi, Y_1(\pm\pi))$ and $Q_{\pm\pi}^{s,u} = (\pm\pi, \bar{Y}_1(\pm\pi))$: we claim that no part of the ∞ -isocline intersects the line $Y_1 = \frac{1}{2} \ln \tilde{\mathcal{A}}$. For $|X| < \frac{\pi}{2}$, we have $Y_1^*(X) < \bar{Y}_1(X) < \frac{1}{2} \ln \tilde{\mathcal{A}}$, and relation (65) implies that

$$\bar{Y}_1(X) < \bar{Y}_1\left(\pm\frac{\pi}{2}\right) = -\frac{k\mathfrak{c}}{\gamma_1} < \frac{1}{2} \ln \tilde{\mathcal{A}}, \quad \text{for all } |X| < \frac{\pi}{2}.$$

For $|X| \in (\frac{\pi}{2}, \pi]$, $\bar{Y}_1^*(X) > Y_1^+(X) > \frac{1}{2} \ln \tilde{\mathcal{A}}$, where the last inequality follows from (56). It remains to show that $\bar{Y}_1(X) < \frac{1}{2} \ln \tilde{\mathcal{A}}$ for $|X| \in (\frac{\pi}{2}, \pi]$. Condition (63) implies that $\bar{Y}_1(\pi) < \frac{1}{2} \ln \tilde{\mathcal{A}}$, and the result follows since we have previously established that $\bar{Y}_1(X)$ is an increasing function on $|X| \in (\frac{\pi}{2}, \pi]$.

To determine the nature of the singular points, at $Q_\pi^{s,u} = (\pi, \bar{Y}_1^*(\pi))$ we have

$$D^2 H_1(\pi, \bar{Y}_1^*(\pi)) = \begin{pmatrix} M_1 g(\bar{Y}_1^*(\pi)) & 0 \\ 0 & -M_1 g(\bar{Y}_1^*(\pi)) - \gamma_1 \end{pmatrix},$$

where the first term in the diagonal is negative, since $\frac{1}{2} \ln \tilde{\mathcal{A}} < \bar{Y}_1^*(\pi)$ and $M_1 < 0$, while the second diagonal term is positive since $\frac{\partial F}{\partial Y_1}(\pi, \bar{Y}_1^*(\pi)) > 0$. Hence Morse theory implies that $Q_{\pm\pi}^{s,u} = (\pm\pi, \bar{Y}_1^*(\pm\pi))$ are saddle points. For $Q_\pi^{s,l} = (\pi, \bar{Y}_1(\pi))$, we get

$$D^2 H_1(\pi, \bar{Y}_1(\pi)) = \begin{pmatrix} M_1 g(\bar{Y}_1(\pi)) & 0 \\ 0 & -M_1 g(\bar{Y}_1(\pi)) - \gamma_1 \end{pmatrix},$$

and we note that the first term on the diagonal is positive, since $F(X, \cdot)$ is convex, $M_1 < 0$ and $\bar{Y}_1(\pi) < \frac{1}{2} \ln \tilde{\mathcal{A}}$, while the second diagonal term is negative since F is decreasing at $(\pi, \bar{Y}_1(\pi))$. Thus, $Q_{\pm\pi}^{s,l} = (\pm\pi, \bar{Y}_1(\pm\pi))$ are saddle points as well. For $Q_0^c = (0, \bar{Y}_1(0))$,

$$D^2 H_1(0, \bar{Y}_1(0)) = \begin{pmatrix} -M_1 g(\bar{Y}_1(0)) & 0 \\ 0 & M_1 g(\bar{Y}_1(0)) - \gamma_1 \end{pmatrix},$$

the first diagonal term is negative since $\bar{Y}_1(0) < \frac{1}{2} \ln \tilde{\mathcal{A}}$ and $F(0, \cdot)$ is concave, while the second diagonal term is also negative since $Y_1^+(0) < \bar{Y}_1(0)$ and F is decreasing at $(0, \bar{Y}_1(0))$. Thus, Morse theory implies that $Q_0^c = (0, \bar{Y}_1(0))$ is a centre.

For $Q_0^s = (0, Y_1^*(0))$ then

$$D^2 H_1(0, Y_1^*(0)) = \begin{pmatrix} -M_1 g(Y_1^*(0)) & 0 \\ 0 & M_1 g(Y_1^*(0)) - \gamma_1 \end{pmatrix},$$

then the first diagonal term is negative since $Y_1^*(0) < \frac{1}{2} \ln \tilde{\mathcal{A}}$, while $Y_1^*(0) < Y_1^+(0)$ implies that the second diagonal term is positive, hence $Q_0^s = (0, Y_1^*(0))$ is a saddle point. \square

Remark 4.11. *The saddle point $Q_0^s = (0, Y_1^*(0))$ which lies below the streamline of the surface wave (in terms of (X, Y_1) coordinates) is equivalent to $F(0, -\epsilon_1) > 0$, due to the monotonicity of $F(0, \cdot)$ and, similarly, the saddle points $Q_{\pm\pi}^{s,u} = (\pm\pi, \bar{Y}_1^*(\pm\pi))$ lying above the streamline of the internal wave in (X, Y_1) coordinates is equivalent to $F(\pm\pi, kh_1 + \epsilon) < 0$.*

Remark 4.12. *In the case where the inequality (63) does not hold then, for some $X_0 \in (\frac{\pi}{2}, \pi)$, we have*

$$F\left(X_0, \frac{1}{2} \ln \tilde{\mathcal{A}}\right) = 0 \iff M_1 \cos X_0 \sqrt{A^2 - 1} = k\epsilon + \gamma_1 \frac{1}{2} \ln \tilde{\mathcal{A}}.$$

It follows that there are 8 singular points for system (36). These additional points are located at $(\pm X_0, \frac{1}{2} \ln \tilde{\mathcal{A}})$ which lie at the intersection of the branch of the ∞ -isocline given by the graph of \bar{Y}_1 , and the horizontal part of the 0 -isocline given by $Y_1 = \frac{1}{2} \ln \tilde{\mathcal{A}}$. It can be easily verified that the Hessian matrices (39) for H_1 , evaluated at these points, have zero eigenvalues.

5 Discussions and conclusions

In this paper we employed a phase plane analysis to determine qualitative features of the underlying flow for coupled periodic surface and internal waves, in a two-layer fluid model with (constant) vorticity. The inclusion of rotational effects in the upper fluid layer represents a significant departure from the recent analyses in [20, 21], with the vorticity $\gamma_1 \neq 0$ complicating all aspects of the resulting wave field kinematics. Although the waves being analysed are linear in the fluid dynamics sense — that is, they are of (relatively) small amplitude and steepness — the resulting dynamical systems (31a) and (31b) which govern the motion are themselves fully nonlinear.

We have shown that, similarly to [20, 21], the value of the non-dimensional parameter A plays an overarching role in the configuration of the flow dynamics and, in particular the number, and location, of singular points. However, unlike for the irrotational case (cf. [19]), the inclusion of vorticity permits the possibility that A is less than 1, and indeed it may attain negative values. Disparate qualitative behaviour is observed for the three regimes: $|A| < 1$, $A = 1$, $A > 1$, respectively. In each of these regimes we show that three qualitatively different flow formulations may arise, depending on whether there are critical layers in the flow interior (for $\mathfrak{c} = c - \gamma_1 h_1 < 0$), or not (when $\mathfrak{c} > 0$), with the latter scenario having two different possible flow configurations depending on whether the vorticity γ_1 is positive, or negative.

In this paper we construct detailed qualitative depictions of the streamlines for the different possible flows in the steady moving frame. In so doing, we are undertaking an analysis of the flow dynamics from the Eulerian perspective of a fixed-observer. A natural follow-on to this will be to use these results in order to obtain a qualitative understanding of individual particle motion, as was done for the much simpler irrotational setting in [20, 21]. Translating the results of this paper to such a Lagrangian framework for rotational flows is currently work in progress. Additionally, we have set the vorticity to zero in the bottom fluid layer for the purposes of expediency, and since a rotational upper layer is of greater interest both mathematically and physically. Recent work in [6, 7, 8] has constructed Hamiltonian frameworks describing the evolution of internal waves in the two fluid layer model

where both fluid layers possess a sheared current. An interesting extension of this paper would be to consider the underlying flow for coupled surface and internal waves whereby the lower fluid layer possesses (constant) vorticity.

Appendix: Limiting values of the parameter A

In the recent paper [19] it is proven that $A = A(h, h_1, k) \geq 1$ in the irrotational setting ($\gamma_1 = 0$). This result follows from determining the asymptotic values of A with respect to k (without loss of generality), and establishing monotonicity properties for $A(k)$. In Remark 3.2 and Lemma 3.1 we stated that richer, and more complex, behaviour is exhibited by the parameter $A = A(h, h_1, k, \gamma_1)$ in the rotational setting ($\gamma_1 \neq 0$), as we now discuss.

For the purpose of illustration, and simplicity, we consider the behaviour of $A = A(k)$ as it varies with respect to k alone. Firstly, we recall that

$$A(k) = \frac{g - \gamma_1[c(k) - \gamma_1 h_1]}{k[c(k) - \gamma_1 h_1]^2} = \frac{g - \gamma_1 \mathfrak{c}(k)}{k \mathfrak{c}(k)^2}, \quad \mathfrak{c}(k) := c(k) - \gamma_1 h_1, \quad (66)$$

where $c(k)$ is given by the solution of the fourth order dispersion relation (30). One can check that the solutions $c(k)$ are even functions of k , and thus $A(k)$ is an odd function of k : hence we consider only positive values of k .

To investigate asymptotic behaviour in the short-wave limit, $\lim_{k \rightarrow \infty} A(k)$, we note that $\tanh(kh) \rightarrow 1$ exponentially fast, while terms of the form $1/(kh_1)$ have a polynomial decay of the order -1 . Replacing $\tanh(kh)$ and $\tanh(kh_1)$ by 1 in (30), this relation can then be explicitly solved to get asymptotic short-wave expressions for $c(k)$:

$$c_{1,2}(k) \simeq \gamma_1 h_1 + \frac{-\gamma_1 \pm \sqrt{4gk + \gamma_1^2}}{2k}, \quad (67)$$

$$c_{3,4}(k) \simeq \gamma_1 h_1 + \frac{-2\gamma_1 h_1 k(r+2) + \gamma_1 \pm \sqrt{4gkr(r+2) + \gamma_1^2}}{2k(2+r)}. \quad (68)$$

The solutions $c_{1,2}$ correspond to barotropic (surface) wave modes, whereas $c_{3,4}$ correspond to the baroclinic (internal) wave modes. Then, from (66) with (67) and (68) one gets

$$\lim_{k \rightarrow \infty} A_{1,2}(k) = 1, \quad \lim_{k \rightarrow \infty} A_{3,4}(k) = 0.$$

Hence both $A(k) > 1$ and $A(k) \leq 1$ are possible when $\gamma_1 \neq 0$. This contrasts with the irrotational case ($\gamma_1 = 0$) whereby we obtain the familiar asymptotic expressions (cf. [29])

$$c_{1,2}(k) \simeq \pm \sqrt{\frac{g}{k}}, \quad c_{3,4}(k) \simeq \pm \sqrt{\frac{gr}{k(2+r)}},$$

and $\lim_{k \rightarrow \infty} A_{1,2}(k) = 1$, and $\lim_{k \rightarrow \infty} A_{3,4}(k) = \frac{g}{kc_{3,4}^2} = 1 + \frac{2}{r} > 1$. Since one can prove in the irrotational case that the solutions $A(k)$ decrease monotonically from ∞ to the above limits [19], it follows that $A(k) \geq 1$ always.

In the long-wave limit $k \rightarrow 0^+$, the wave speeds are the roots of the equation

$$c^4 - \gamma_1 h_1 c^3 - g(h + h_1)c^2 + g\gamma_1 h h_1 c + \frac{g^2 r h h_1}{1+r} = 0. \quad (69)$$

It follows from (66) (see Lemma 3.1) that \mathbf{c} (and hence c) is real-valued when $A \geq -\frac{\gamma_1^2}{4gk} \xrightarrow{k \rightarrow 0} -\infty$. Since (69) has constant real coefficients, its roots will have finite constant values, say $c(0)$, and so $\lim_{k \rightarrow 0^+} A(k) = \pm\infty$ for any solution of (69), where the sign matches that of $\text{sgn}[g + \gamma_1^2 h_1 - \gamma_1 c(0)]$. This can be either positive or negative: for large values of h , the surface modes $c \approx \pm\sqrt{g(h + h_1)}$ take values larger than $\frac{g}{\gamma_1} + \gamma_1 h_1$ for

$$h \gtrsim h_0 := \frac{(g + \gamma_1^2 h_1)^2}{g\gamma_1^2} - h_1 = h_1 + \frac{g^2 + \gamma_1^4 h_1^2}{g\gamma_1^2} \geq h_1 + 2h_1 = 3h_1.$$

A degenerate case exists for $c(0) = \gamma_1 h_1$, which is possible if and only if

$$\gamma_1 = \pm \frac{\sqrt{(1+r)grh}}{(1+r)h_1},$$

in which case the limit is clearly $\lim_{k \rightarrow 0^+} A(k) = \infty$.

Acknowledgements

This publication has resulted from research conducted with financial support for DH, RI and ZS from *Research Ireland* under grant number 21/FFP-A/9150.

References

- [1] Ricardo Barros and José Felipe Voloch. Effect of variation in density on the stability of bilinear shear currents with a free surface. *Physics of Fluids*, 32(2), 2020.
- [2] Adrian Constantin. The trajectories of particles in Stokes waves. *Invent. Math.*, 166(3):523–535, 2006.

- [3] Adrian Constantin. *Nonlinear water waves with applications to wave-current interactions and tsunamis*, volume 81 of *CBMS-NSF Regional Conference Series in Applied Mathematics*. Society for Industrial and Applied Mathematics (SIAM), Philadelphia, PA, 2011.
- [4] Adrian Constantin. Particle trajectories in extreme Stokes waves. *IMA J. Appl. Math.*, 77(3, SI):293–307, 2012.
- [5] Adrian Constantin. The flow beneath a periodic travelling surface water wave. *J. Phys. A*, 48(14), 2015.
- [6] Adrian Constantin and Rossen I. Ivanov. A Hamiltonian approach to wave-current interactions in two-layer fluids. *Phys. Fluids*, 27(8):086603, 2015.
- [7] Adrian Constantin and Rossen I. Ivanov. Equatorial wave-current interactions. *Comm. Math. Phys.*, 370(1):1–48, 2019.
- [8] Adrian Constantin, Rossen I. Ivanov, and Calin I. Martin. Hamiltonian formulation for wave-current interactions in stratified rotational flows. *Arch. Ration. Mech. Anal.*, 221(3):1417–1447, 2016.
- [9] Adrian Constantin and Walter Strauss. Exact steady periodic water waves with vorticity. *Communications on Pure and Applied Mathematics*, 57(4):481–527, 2004.
- [10] Adrian Constantin, Walter Strauss, and Eugen Vărvărcă. Global bifurcation of steady gravity water waves with critical layers. *Acta Mathematica*, 217:195–262, 2016.
- [11] Adrian Constantin and Gabriele Villari. Particle trajectories in linear water waves. *J. Math. Fluid Mech.*, 10(1):1–18, 2008.
- [12] Robert M Corless, Gaston H Gonnet, David EG Hare, David J Jeffrey, and Donald E Knuth. On the Lambert W function. *Advances in Computational mathematics*, 5:329–359, 1996.
- [13] Walter Craig, Philippe Guyenne, and Henrik Kalisch. Hamiltonian long-wave expansions for free surfaces and interfaces. *Comm. Pure Appl. Math.*, 58(12):1587–1641, 2005.
- [14] AF Teles Da Silva and DH Peregrine. Steep, steady surface waves on water of finite depth with constant vorticity. *Journal of Fluid Mechanics*, 195:281–302, 1988.

- [15] Mats Ehrnström, Joachim Escher, and Gabriele Villari. Steady water waves with multiple critical layers: interior dynamics. *J. Math. Fluid Mech.*, 14(3):407–419, 2012.
- [16] Mats Ehrnström and Gabriele Villari. Linear water waves with vorticity: rotational features and particle paths. *J. Differential Equations*, 244(8):1888–1909, 2008.
- [17] David Henry. The trajectories of particles in deep-water Stokes waves. *Int. Math. Res. Not.*, pages Art. ID 23405, 13, 2006.
- [18] David Henry. On the deep-water Stokes wave flow. *Int. Math. Res. Not.*, pages Art. ID rnm 071, 7, 2008.
- [19] David Henry, Rossen I. Ivanov, and Gabriele Villari. Flow kinematics for Equatorial coupled surface and internal waves. *Differential Integral Equations*, to appear.
- [20] David Henry and Gabriele Villari. Flow underlying coupled surface and internal waves. *Journal of Differential Equations*, 310:404–442, 2022.
- [21] David Henry and Gabriele Villari. Flow dynamics for coupled surface and internal deep-water waves. *Annali di Matematica Pura ed Applicata*, 202(2):711–736, 2023.
- [22] R.S. Johnson. *A Modern Introduction to the Mathematical Theory of Water Waves*. Cambridge University Press, 1997.
- [23] Blair Kinsman. *Wind Waves: Their Generation and Propagation on the Ocean Surface*. Prentice-Hall, Englewood Cliffs, N.J., 1965.
- [24] Tony Lyons. Particle trajectories in extreme Stokes waves over infinite depth. *Discrete Contin. Dyn. Syst.*, 34(8):3095–3107, 2014.
- [25] Calin Iulian Martin and Bogdan-Vasile Matioc. Gravity water flows with discontinuous vorticity and stagnation points. *Communications in Mathematical Sciences*, 14(2):415–441, 2016.
- [26] James D. Meiss. *Differential dynamical systems*, volume 14 of *Mathematical Modeling and Computation*. Society for Industrial and Applied Mathematics (SIAM), Philadelphia, PA, 2007.
- [27] John Milnor. *Morse theory*. Based on lecture notes by M. Spivak and R. Wells. Annals of Mathematics Studies, No. 51. Princeton University Press, Princeton, N.J., 1963.

- [28] Victor V Prasolov. *Polynomials*, volume 11. Springer Science & Business Media, 2004.
- [29] Bruce R. Sutherland. *Internal Gravity Waves*. Cambridge University Press, 2010.
- [30] GP Thomas and G Klopman. Wave-current interactions in the near shore region. *International series on advances in fluid mechanics*, 10:255–319, 1997.